Seismic characterization of Vlieland Sandstone in the Broad Fourteens Basin – Insights from a new OBN survey

Internship Report

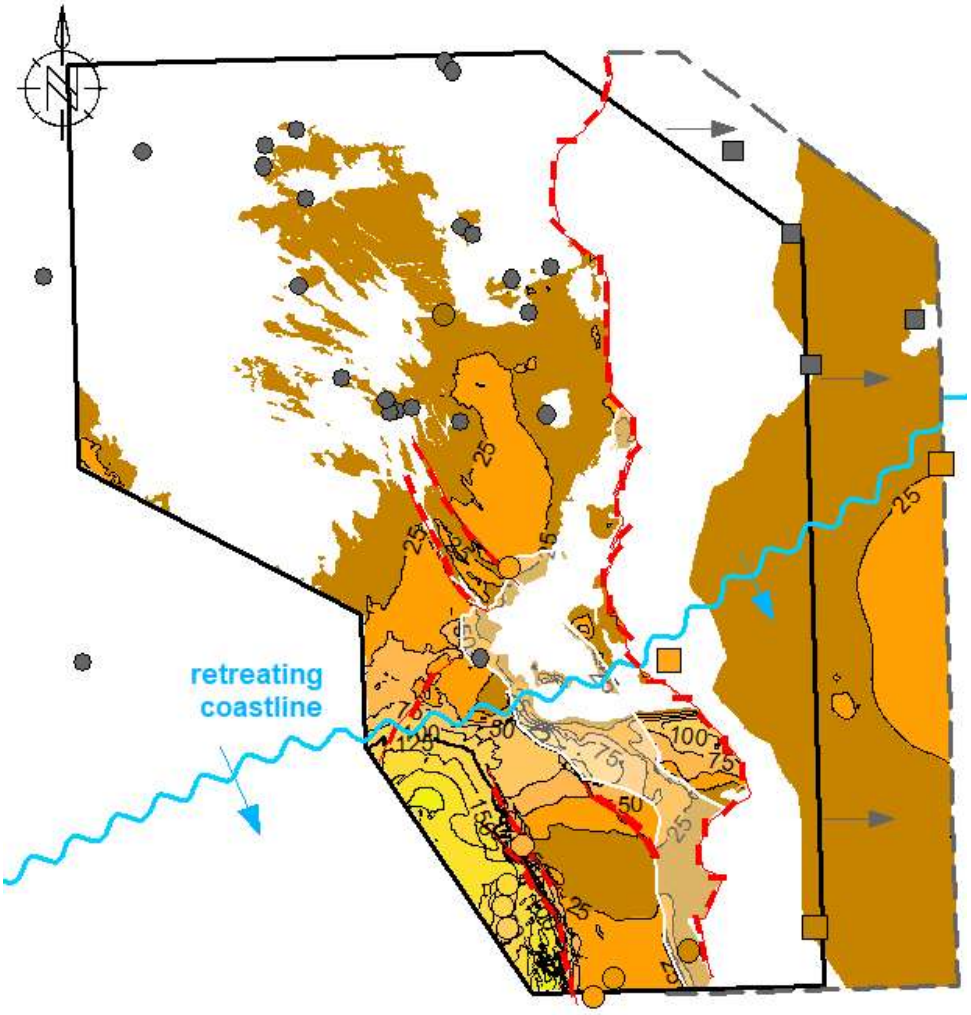

Rozemarijn Das
Student Earth Structure & Dynamics
6898513

EBN Supervisor: Anke Pots
UU Supervisor: Fred Beekman

None of this work would have been possible without the kind permission of: EBN B.V., ONE-Dyas B.V., RockRose (NL) CS1 B.V., Tenaz Energy Netherlands B.V., Wintershall Noordzee B.V., who all provided kind permission to access and share the OBN seismic data used in this study.

Summary

Understanding the spatial distribution of the Vlieland Sandstone Formation, which is part of the Lower Cretaceous Vlieland Subgroup, is of increasing relevance due to subsurface storage needs for CO^2 and hydrogen. This study investigates seismic characteristics of the Vlieland Sandstone formation along the northeastern bounding fault of the Broad Fourteens Basin (BFB), using newly acquired high-resolution Ocean Bottom Node (OBN) seismic data. A synthesis of relevant literature shows that the Vlieland Subgroup is the marine part of a SSE-directed transgression widely recognized in wells in the Dutch subsurface. This transgression followed Cimmerian rifting; the Vlieland Subgroup filled and outstepped the Cimmerian basins. In the Late Cretaceous followed a phase of compression, during which the northeastern bounding fault of the BFB was inverted. An E-W panel across the research area was created, highlighting major differences in stratigraphic completeness across the bounding fault. A N-S panel in the BFB demonstrates that variations in sandstone thickness are related to the transgression direction and to fault-governed accommodation space, also considering the biostratigraphy showing that the Base and Top Vlieland Subgroup are time-equivalent. Ten synthetic seismograms were generated to characterize seismic impedance contrasts at key Vlieland interfaces. The Top Vlieland Subgroup is consistently mappable across the research area. The Base Vlieland Subgroup can be followed relatively well in the basin – despite variable subcrop – yet on the platform high interpretation uncertainty required assumptions guided by the Top Vlieland Subgroup surface. The Top Vlieland Sandstone seismic character proved highly variable, limiting its traceability, especially across faults. Given these challenges, an empirical relationship between well top thickness of Vlieland Sandstone and the total Vlieland Subgroup was established (R^2 = 0.88). In the basin, the predicted Top Sandstone surface fits well with interpretations on seismic. This enabled the construction of seismics-informed Gross Depositional Environment (GDE) map for the full research area, with local prediction of Vlieland Sandstone thickness. Results in map view fit with well panel observations that sandstone distribution is controlled both by SSE-directed transgression and by subordinate faults on the BFB main bounding fault. Acknowledging uncertainties, the GDE map could be offers a first-order guidance for evaluating Vlieland Sandstone thickness along the northeastern BFB bounding fault. Uncertainties lie in the empirical rather than causal nature of the model, in Base Vlieland interpretation and in the unknown Net-to-Gross ratio of the modeled sand thickness.

Contents

1. Introduction

The perspective on the geological exploitation of the Dutch offshore has shifted, driven by an increasing urgence for CO_2 and H_2 storage (e.g. KGG, 2025; Lau et al., 2021) as part of the energy transition. This shift calls for an improved understanding of the storage capacity of all potential reservoirs that lie beneath the Dutch North Sea. Factors influencing whether fluids or gases can be stored in a subsurface reservoir, include the presence of: I) a reservoir rock, which can hold fluid or gas due to its porosity and permeability; II) a seal rock, which 'caps' the reservoir, preventing fluids from escaping upward due to its lack of permeability and III) a trapping system, which provides a three-dimensional arrangement of the reservoir- and seal rocks to capture fluid or gas (Head & Simmons, 2020). If any of these components are absent, effective trapping is not possible. In this context, the Lower Cretaceous Vlieland Sandstone formation requires detailed understanding. In some parts of the Dutch offshore, this formation subcrops the widely present Vlieland Claystone formation. The presence, thickness and permeability of the Vlieland Sandstone, determines whether the lowermost Vlieland Subgroup is suitable for storage.

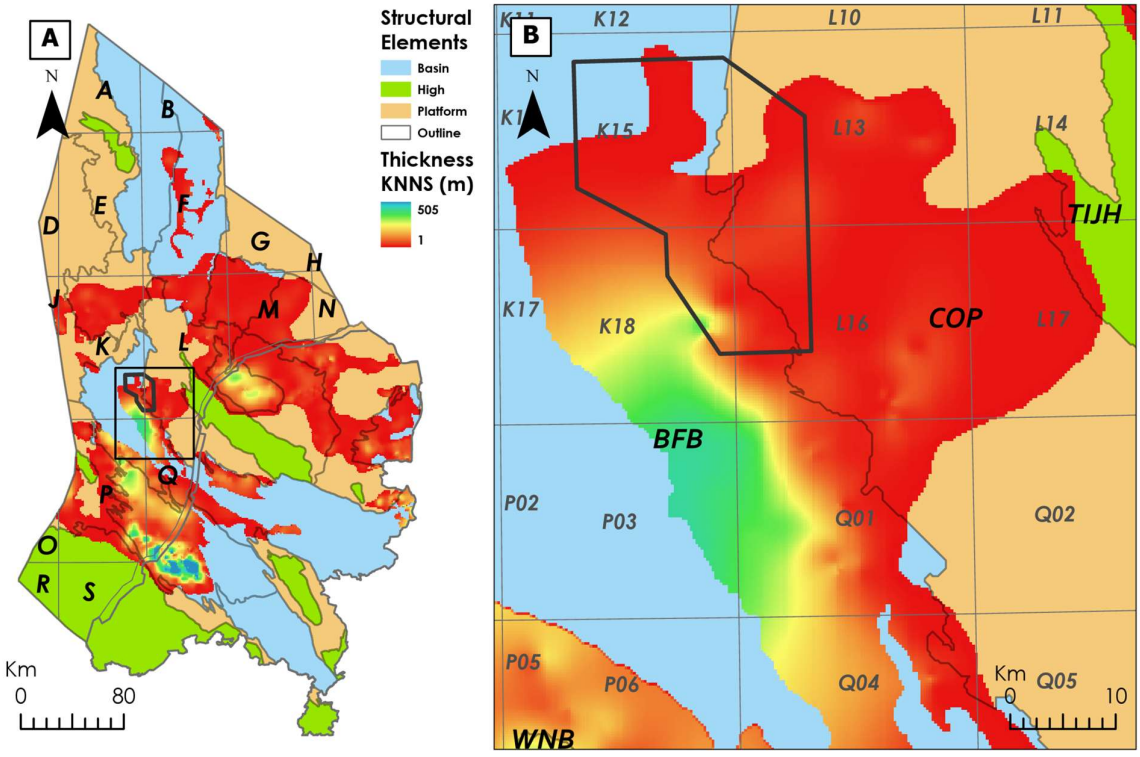

Figure 1: A) Aggregated thickness of Vlieland Sandstone members adapted from GEODE-ATLAS (Ten Veen et al., 2023), with overview of the structural elements of the Netherlands from Kombrink et al.(2014), B) Zoom-in to map A. Black polygon indicates the OBN-survey area. BFB = Broad Fourteens Basin, COP = Central Offshore Platform, TIJH = Texel-Ijsselmeer High, WNB = West Netherlands Basin.

1.1 Problem Definition

The variable geological characteristics of the Vlieland Subgroup present a significant challenge for assessing the potential for fluid or gas storage. The Vlieland Subgroub comprises two formations. The youngest formation is the Vlieland Claystone Formation (KNNC), which often is present in Dutch on- and offshore stratigraphy. Locally, below KNNC, is the older Vlieland Sandstone Formation (KNNS), which is deposited in the Netherlands in different basins as different members (TNO - GDN, 2025) (Fig. 1A). The Vlieland Subgroup records the marine part of a Late Jurassic to Early Cretaceous transgression. The transgression flooded a large area: from this age, sediments indicative of relative sea level rise are found in numerous wells in the Dutch on- and offshore (Jeremiah et al., 2010).

The seismic character of the onset of transgression is hard to characterize for various reasons. Firstly, the subcropping units vary laterally. In the area of interest, the onset of the transgression is generally set at the Late Cimmerian Unconformity (LCU). The LCU can coincide in some places, mostly on highs, with the more pronounced Mid Cimmerian Unconformity (MCU). The unconformities cut into underlying strata at different stratigraphic levels - from the continental deposits (Late Jurassic) below, down to locally even the Carboniferous Limburg Group. Where the unconformities do not coincide, e.g. in parts of the Broad Fourteens Basin (BFB), West Netherlands Basin (WNB) and Dutch Central Graben (DCG), continental deposits of the Late Jurassic to Earliest Cretaceous are preserved (Bouroullec et al., 2024). Secondly, the base of the Vlieland, i.e. the supracropping lithology also varies laterally: either Vlieland Sandstone might be at the base of the Vlieland Subgroup, or the Vlieland Claystone formation. The thirteen different members of the Vlieland Sandstone Formation comprise a wide variety of depositional environments and lithologies, from massive shoreface sandstones (e.g. Kotter, Helder) to calcareous shell-bearing coastal to offshore sandstones (onshore Vlieland) (Verreussel et al., 2025). Within one basin, multiple sandstone members can be present, implying lateral variability even on the basin scale (Den Hartog Jager, 1996; Willems et al., 2020). On top of this, the thickness of the Vlieland Sandstone Formation is also highly variable; when its thickness is below seismic resolution, characterizing its presence becomes even more complex.

1.2 Project Objectives

The objective of this study is to gain a more detailed understanding of the spatial distribution and properties of the Vlieland Subgroup, with emphasis on the presence and character of the Vlieland Sandstone members potentially suitable for storage applications. Where no Vlieland Sandstone is present, the Vieland Subgroup functions as a seal, being only represented by the Vlieland Claystone formation. Conversely, when the Vlieland Sandstone is present, the sandy units can form either a ‘thief zone’ into which fluids or gases might migrate upwards from a reservoir below, or it may form a reservoir by itself, with the Vlieland Claystone acting as a seal. Which impact the Vlieland Sandstone will have on storage potential – from a reservoir below or from a reservoir in the Vlieland Sandstone Formation – naturally depends on the porosity and permeability of the sandstones, and on their thickness.

Due to the high variability of the Vlieland Sandstone Formation, the unit must be analyzed at a smaller scale. Therefore, in this study, a systematic analysis will be performed just below basin-scale, along the northeastern bounding fault of the Broad Fourteens Basin (BFB), starting at a portion of the fault in the K15, K18, L13 and L16 blocks (Fig. 1B, Fig. 2). This area is considered suitable for such detailed analysis, as novel and high resolution Ocean Bottom Node (OBN) data are available for this area, obtained using state-of-the-art acquisition and processing techniques (Chaves et al., 2011). The increased seismic illumination and penetration compared to legacy seismic data (Presentations DXD, 2024) may allow for new insights on the geological structure of the area and the seismic expression of Vlieland Sandstone.

The objectives of this project will be tackled in a three-fold workflow, each part associated with specific deliverables. Firstly, existing well-data, 2D and 3D horizon interpretations and existing reports on the area will be collected to map available resources and to define remaining knowledge gaps. Previous studies on the Vlieland Sandstone Formation and the BFB will be summarized to gain a comprehensive understanding of the geological setting, to provide context for following steps. Secondly, wells containing Vlieland Sandstone will be analyzed to characterize and correlate the different Vlieland Sandstone members based on e.g. gamma-ray, density and sonic logs. The latter two logs will be used to produce synthetic well logs: expected seismic response of the Vlieland Subgroup will be calculated for eight wells. Thirdly, for the Vlieland Subgroup and Vlieland Sandstone Formations, top and base horizons will be interpreted on seismic. Horizon interpretation will be supported by fault mapping, seismic-to-well ties, and will be performed with consideration of the area's structural history. Using well characterization and correlation, together with insights gained from seismic interpretation, a Gross Depositional Environment (GDE) map will be constructed. The GDE map will have the primary goal of illustrating the Vlieland Sandstone thickness distribution in the research area, together with factors that influence Vlieland Sandstone thickness distribution here.

2. Background

2.1 Geological Framework

2.1.1 Basin Development

The area of interest lies at the edge of the Broad Fourteens Basin (BFB), which is one of the so-called Cimmerian basins in the Netherlands (Fig. 2). Though labeled 'Cimmerian' basin – it formed during the Cimmerian Phase, i.e. in response to the Triassic and Early to Middle Jurassic breakup of Pangaea (Stille, 1926; Ten Veen et al., 2025) – the NW-SE trend of the main bounding faults is likely as old or older than the Variscan London-Brabant Massif (Smit et al., 2018; Woodcock & Strachan, 2015) (Fig. 3).

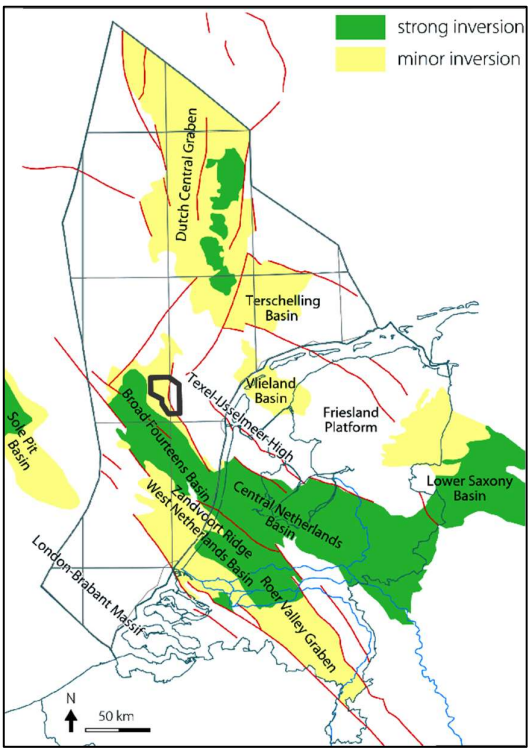

Figure 2: Cimmerian rift basins in the Netherlands and the amount of associated inversion, modified from Ten Veen et al. (2025) and De Jager (2007).

Rifting commenced in the Triassic, with a rift branch developing between Greenland and Scandinavia and propagating southwards. Eventually, another branch to the west would become the main rift; the eastern branch in the Netherlands being a 'failed rift' with cessation of rifting in the Early Cretaceous (Ziegler & Cloetingh, 2004). Evidence for early-stage 'rifting' is in the thicker Triassic sediments in the BFB, WNB and CNB (Central Netherlands Basin) with respect to the surrounding structures (J. Ten Veen et al., 2025). In the Triassic to Early Jurassic, sedimentation occurred under slow, continuous subsidence and facies deepened (e.g. Peeters et al. (2018)). Faulting was limited, but evidence exists for Early to Middle Jurassic normal faulting in the BFB and WNB (J. Ten Veen et al., 2025). Locally, subsidence was influenced by salt tectonics of underlying Zechstein salt, with stronger subsidence where salt was present (De Jager, 2014).

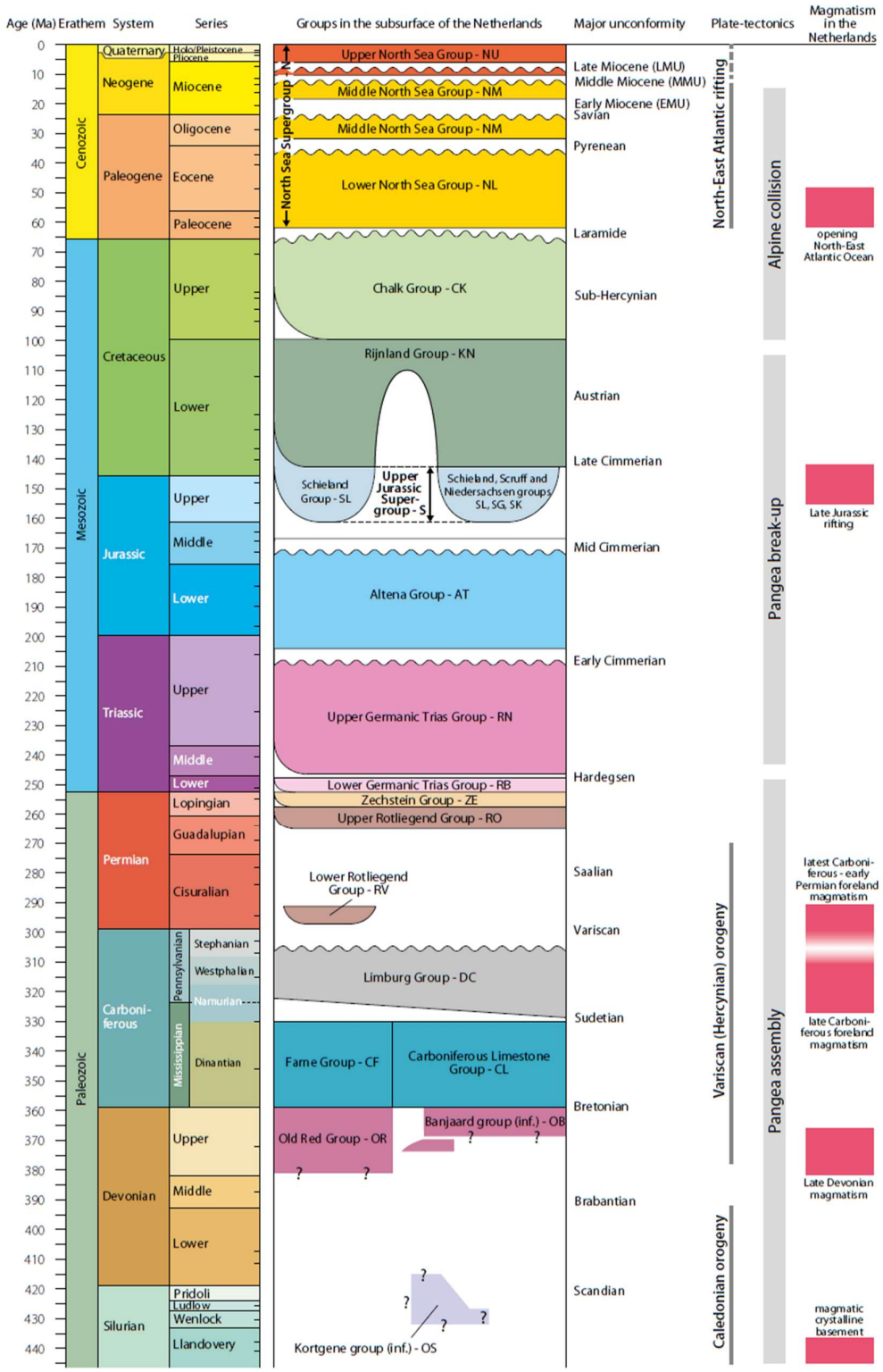

Figure 3: Tectono-Stratigraphic Column applying to the large stratigraphic groups in the Netherlands (J. Ten Veen et al., 2025). The Vlieland Subgroup (stratigraphic code: KNN) is part of the Lower Cretaceous Rijnland Group (KN).

In the Middle Jurassic followed a phase of thermal uplift and low eustatic sea level (Haq, 2018), which caused erosion and non-deposition outside the basins, leading to the Mid-Cimmerian Unconformity (MCU) (J. Ten Veen et al., 2025)(Fig. 3). The main rifting phase, i.e. the phase with the thickest depocenters (<2500

m of clastics) occurred in the Late Jurassic. E-W directed extension expressed itself in the N-S trending normal faults of the northern Dutch offshore. This trend terminated in the NW-SE grain of the mid- to south Netherlands, leading to transtensional development of the BFB and other NW-SE trending basins (Bouroullec et al., 2024). With normal faulting, basins deepened and simultaneously platforms were uplifted, resulting in the deep truncations of the Late Cimmerian Unconformity (LCU) (Fig. 3). Complex stratigraphy developed due to the presence of several sub-basins, each with distinct tectonic and depositional histories, different formations and members. In the BFB, the Schieland Group represents the continental to deltaic syn-rift deposits (see Fig. 3). At Rotliegend level (see Fig. 3), normal faulting created tilted fault blocks that were decoupled from overlying strata by Zechstein salt. In the Early Cretaceous, rifting ceased as continental breakup progressed in a rift branch west of the UK. In a phase of post-rift thermal subsidence that coincide with a cooler, more humid period, relative sea levels rose; this allowed marine waters to enter the Dutch Cimmerian basins from the North (Boogaert & Van Adrichem Kouwe, 1993; Jeremiah et al., 2010; Schneider et al., 2018b, 2018a). Sediments from this transgressive stage belong to the Vlieland Subgroup (Code: KNN), with the Vlieland Sandstone Formation (Code KNNS) representing the transgressive basal sands, prograding coastal-barrier or offshore shoal-sands with different members in each basin.

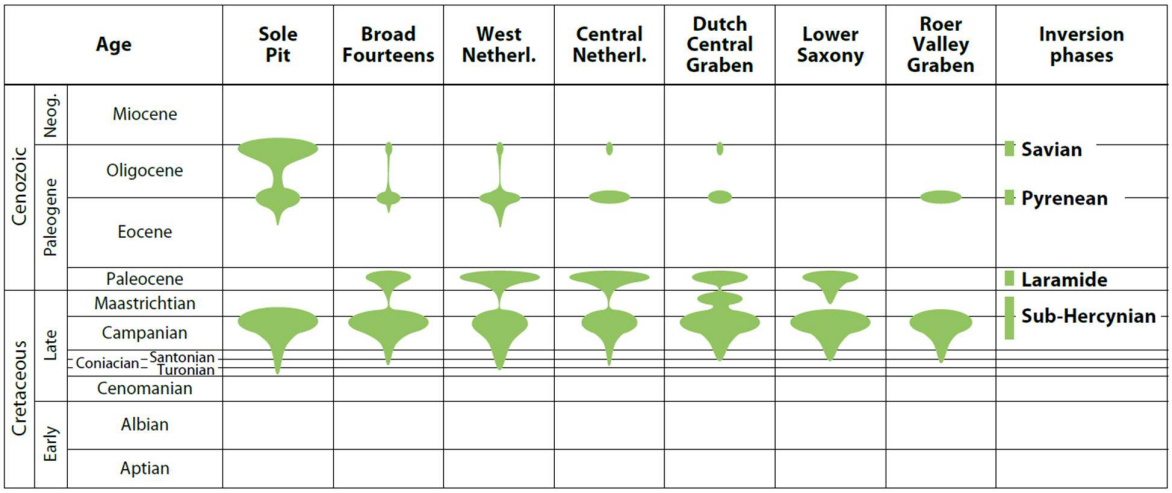

Figure 4: Timing and relative intensity of inversion during pulses of Alpine inversion in the Dutch basins and Sole Pit Basin, modified by J. Ten Veen et al. (2025) from De Jager (2007). Inversion occurred in simultaneous pulses in different basins, but with different magnitudes. The Sub-Hercynian pulse was the large pulse across all Dutch basins.

In the Late Cretaceous, compressional forces took over with the convergent plate movement of the African and European plates (J. Ten Veen et al., 2025). Uplift was continuous but accentuated by pulses of inversion phases (Jager, 2007); the pulses can be linked to convergence rates in the Alpine domain (Deckers & vVan der Voet, 2018). Across multiple basins in the Netherlands, inversion was strongest in the first inversion phase (Sub-Hercynian, see Fig. 4) (De Jager, 2007). The intensity of inversion varied per basin (Fig. 4). Furthermore, the nature of inversion also varied per basin, e.g. it was strongly affected by the presence of Zechstein salt. In the BFB, the influence of salt is demonstrated in the uplift and inversion of Rotliegend-level half grabens decreasing towards the North, correlating with the increase in the thickness of Zechstein salt in this direction. The northeastern bounding fault – which initially developed as a growth fault due to gravitational salt flow – was inversely reactivated during the Laramide phase (Hooper et al., 1995). Salt was initially thought to have acted as decollement during reverse faulting, yet Hooper et al. (1995) demonstrated faulting propagating into the basement underlying the salt. In the BFB and on surrounding platforms, NW-SE trending anticlinal faults developed. In the WNB for example, with relatively thin Zechstein, inversion was expressed as flower structures that formed during the Sub-Hercynian phase. The Pyrenean Phase shows limited inversion of most basins, though overall uplift continued.

Uplift had largely ceased at the end of the Mesozoic, seen from the clear angular unconformity at the base of the North Sea Supergroup. Sediments of the Eridanos river system were deposited near-horizontally, as tectonic activity in The Netherlands largely ceased with exception of the Roer Valley Graben (RVG).

2.1.2 Formation Description

Because of the dynamic tectonic setting, but also due to variable climate conditions, a large array of different depositional environments developed in response to Late Jurassic-Early Cretaceous Cimmerian rifting. Therefore, the stratigraphy is characterized by diachroneity and juxtapositions; this especially holds for the Vlieland Sandstone Formation (see Fig. 5). In each basin, the transgression was expressed differently, which is why KNNS is a collection of members with the same genetics but with different litho- and chronostratigraphy. Below is a detailed description of the stratigraphy in the BFB; note that characteristics in other basins will be different (Verreussel et al., 2025)(Fig. 5).

In earlier work, the Vlieland Subgroup is described as one of five Late Jurassic - Early Cretaceous tectonostratigraphic megasequences (TMS), each megasequence describing genetically related sediment accumulations, deposited in one of the five phases in response to Late Cimmerian rifting (Fig. 6) (Bouroullec et al., 2018; Verreussel et al., 2018). The Schieland Group comprises the first three megasequences, which record syn-rift deposits restricted to the basins only. TMS1 misses in the BFB, but the syn-rift deposits of TMS2 and TMS3 are represented, indicating a shift in extension from E-W to NE-SW (Verreussel et al., 2018; Zanella & Coward, 2003). Thick sediments represent TMS2 in the BFB, with large thickness variations of the syn-rift units due to differential subsidence of half grabens. TMS3 captures the onset of a transition from active rifting to post-rift thermal sag. In the BFB, the onset of TMS3 is erosional in character due to uplift associated with volcanism. Above the erosional surface, lagoonal-marine interfingering is recorded, reflecting the transition to post-rift thermal sag (Fig. 6).

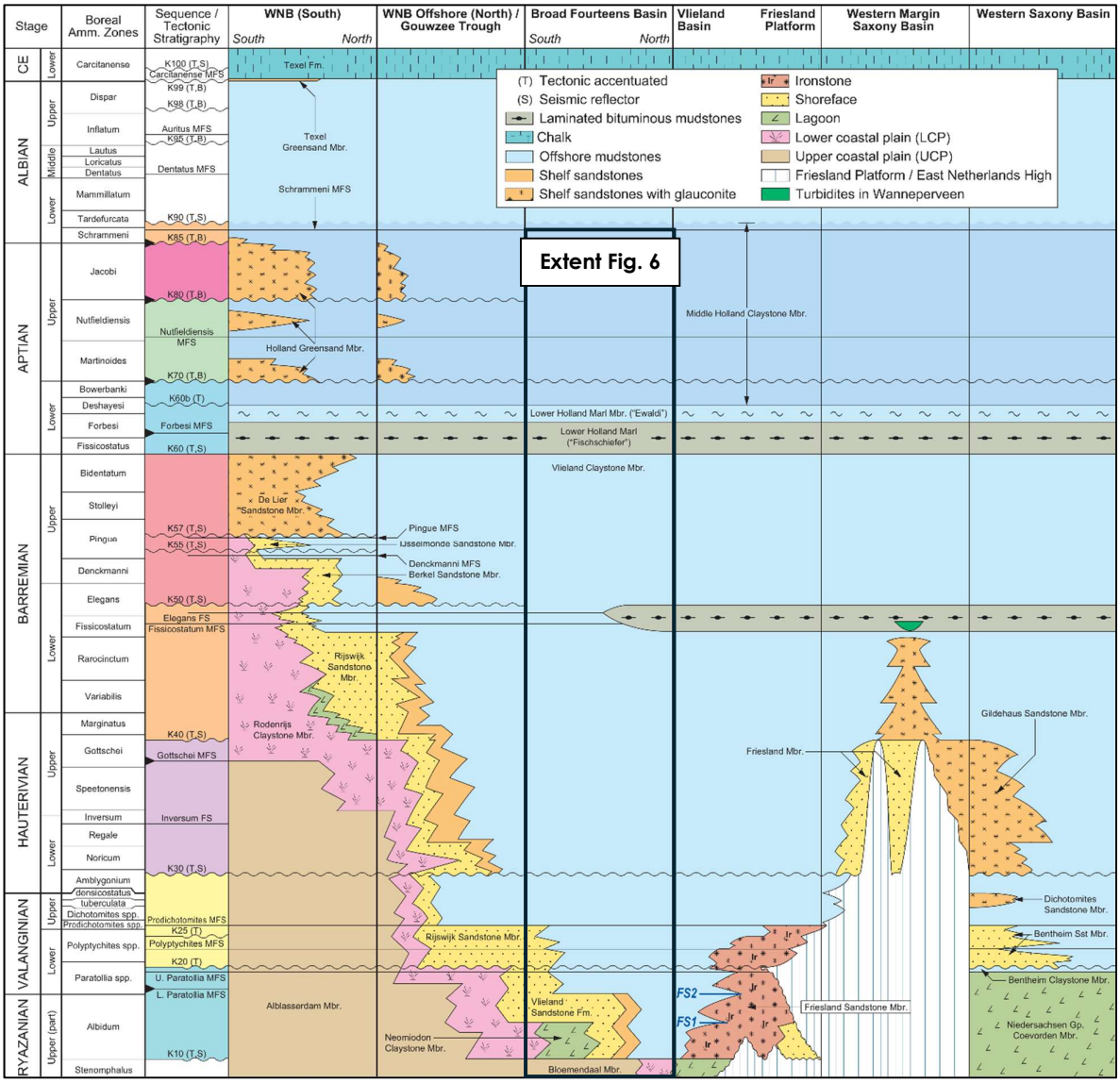

Figure 5: In the Dutch North Sea, the stratigraphic record of the Late Cretaceous interval varies between basins. From: Jeremiah et al. (2010).

The Rijnland Group (Code: KN) comprises TMS4 and TMS5; they record the relatively quiet tectonic phase with relative uniform post-rift subsidence that followed Late Cimmerian Rifting (TNO - GDN, 2025; Verreussel et al., 2025). The youngest unit in in the Rijnland Group is the Vlieland Subgroup (TMS4), which represents marine environment with clastic input. Within the Vlieland Subgroup, the sandstone interval (or in some parts multiple sandstone intervals) belong to the Vlieland Sandstone Formation (Code: KNNS). Characteristic for a thermal sag phase, deposition outstepped the basins; TMS4 and TMS5 are found on platforms and highs, as well. Still, evidence for faulting during Vlieland Subgroup deposition demonstrates that accommodation space was not only created by thermal subsidence (Bouroullec et al., 2024). The more distal part of the transgression is represented by the Vlieland Claystone formation (Code: KNNC), which succeeds KNNS in the BFB. Here, the two formations are laterally equivalent; they represent a trend in the depositional environment from proximal to distal. Throughout the Netherlands, KNNS is subdivided into thirteen members, representing varying depositional environments and ages (Van Adrichem Kouwe & Boogaert, 1993). In the research area, KNNS is represented by thick and massive sandstones of the Helder and Kotter members. The Kotter and Helder members were deposited under shallow marine conditions, in

a shoreface or barrier island depositional environment (Bouroullec et al., 2024; Den Hartog Jager, 1996; Jeremiah et al., 2010). Sediment supply for these sandstones was possibly provided by erosion the rift shoulders of the BFB bounding faults (Verreussel et al., 2025). TMS5 consists of the Holland Formation with a fully marine and sediment-starved environment, far away from major landmass. The base of TMS5 has high gamma ray values, from fossil- and organic-rich shales.

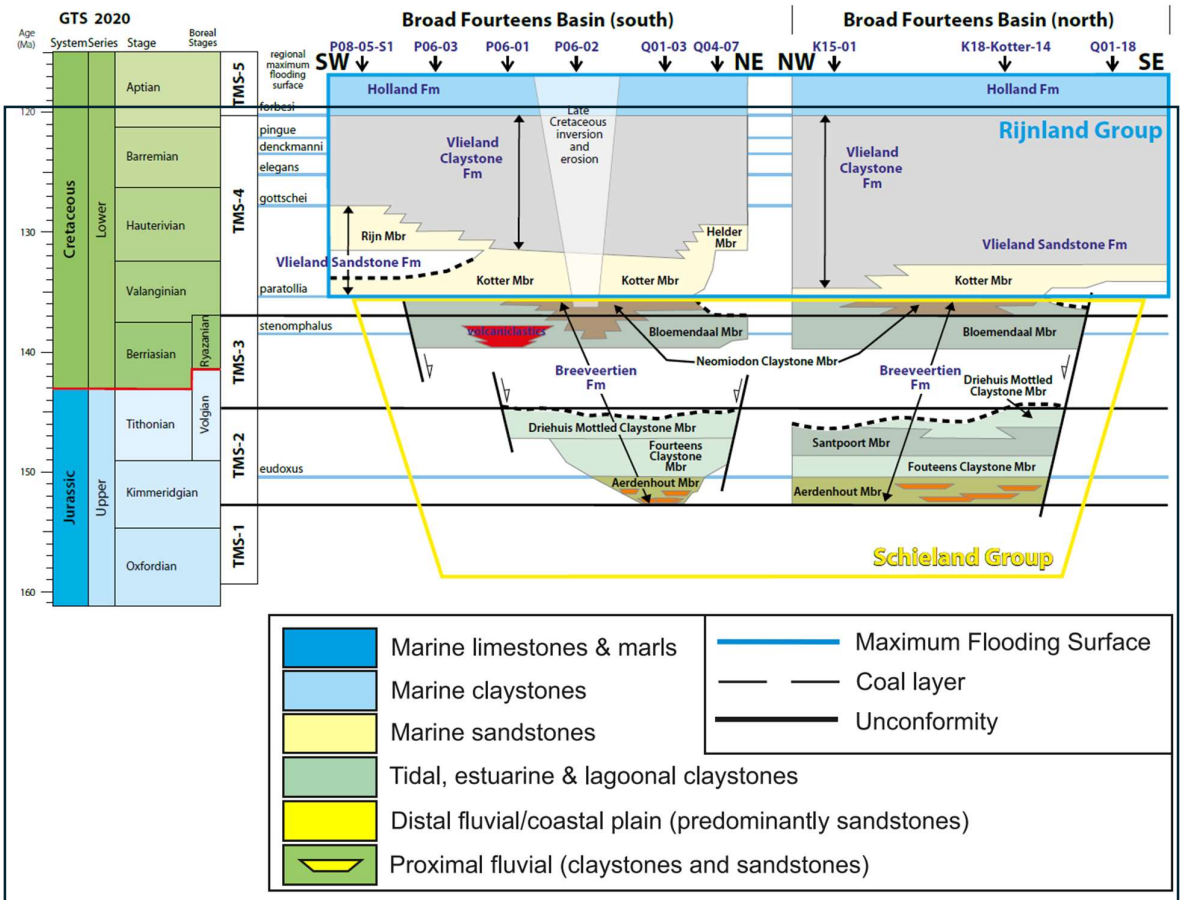

Figure 6: Wheeler diagram of the Broad Fourteens Basin (Bouroullec et al., 2024), indicating the different tectonic megasequences and associated formations. The distinction between the Rijnland Group and Schieland group is not based on age, but on depositional environment. The Rijnland Group is marine, whereas the Schieland Group is continental to fluvial or deltaic.

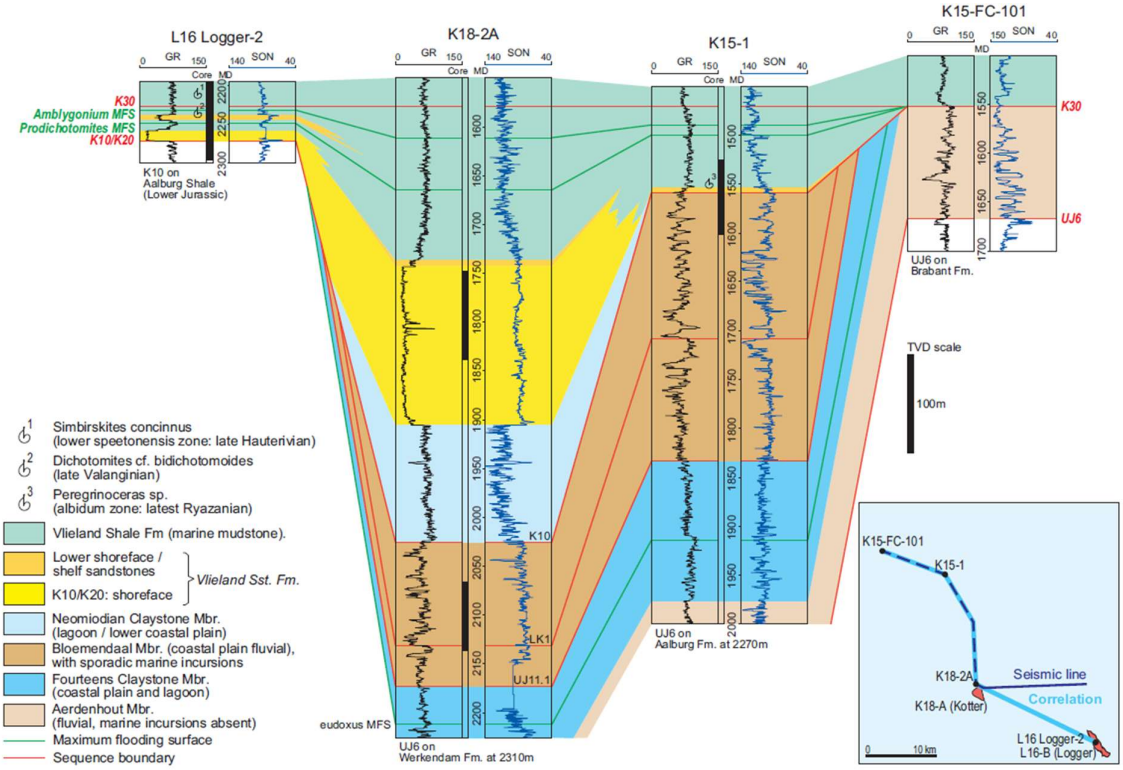

Figure 7: Well correlation panel from key wells in the Northern BFB, from Jeremiah et al. (2010). The thick sandstone deposits in the Kotter well (K18-2A, see also Fig. 6), shales out towards the North, and thins significantly towards the Southeast.

2.2 Context OBN Survey

One of the main reasons for conducting this internship project, is that in 2024 novel seismic data has been acquired on the K15, K18, L13 and L16 blocks. In the OBN-area, multiple 2D and 3D surveys had already been acquired before the OBN survey. However, due to structural complexity in this area, improvements on the imaging quality beyond the legacy surveys were required to derisk potential storage opportunities (Presentations DXD, 2024). Derisking via improved seismic imaging was considered a better option than drilling exploration wells: with a new seismic survey, an entire portfolio of possible reservoirs could be de-risked rather than one single aquifer or depleted reservoir.

For seismic improved illumination and penetration compared to legacy survey, acquisition with large offset (9km), full-azimuth and a broad spectrum was required. These improvements were considered specifically valuable for enhanced imaging of structures below the BFB boundary fault and below Zechstein salt. Hence the proposed acquisition technique was NOAR OBN (Node-ON-A-Rope Ocean Bottom Node, hereafter: OBN). Amongst the parties that collaborated to survey acquisition and processing of were EBN, NAM offshore BV (Nederlandse Aardolie Maatschappij, of which Tenaz Energy Netherlands took operatorship as per May 1st 2025), WINZ (Wintershall Noordzee), Shell, Shearwater GeoServices, Schlumberger, ONE-Dyas and RockRose Energy. From September 2022 to March 2023 acquisition was done; processing took from December 2022 until September 2024. to the complex structural setting, several iterations of the velocity model were performed, resulting in 'Velocity Model K' as the final product. Various types of migration were delivered after the end of the imaging phase of the OBN-survey, but the RTM PreSDM deliverables are preferred for interpretation. The resulting time and depth cubes allow for interpretations that were more reliable than in the past, yet it should be noted that imaging below the BFB bounding fault remains challenging; lateral variations in high-velocity chalk and Zechstein salt explain these challenges.

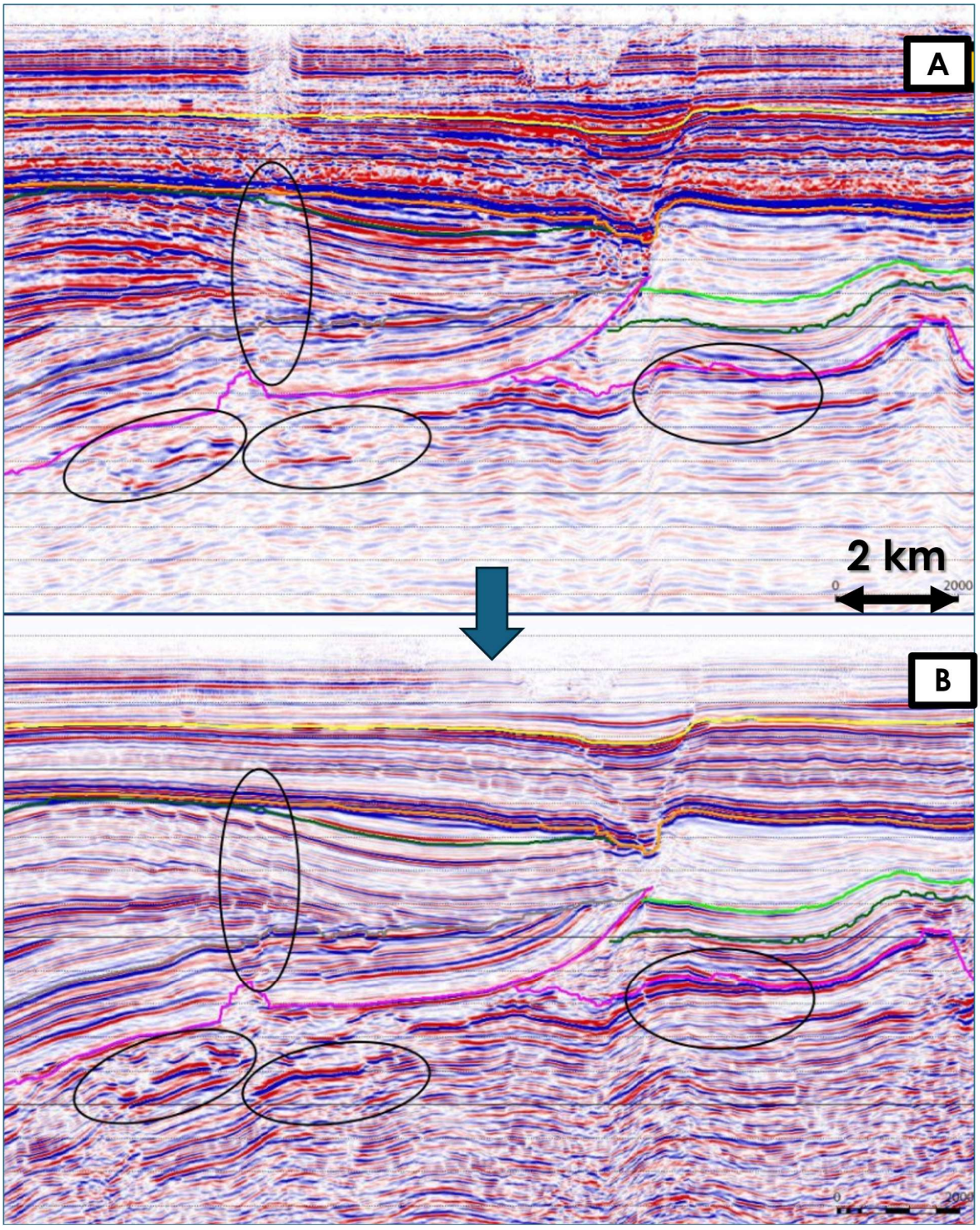

Figure 8: Demonstration of improved imaging, when comparing legacy seismic (A) and OBN seismic (B). The pink line denotes the top Zechstein salt. The two pictures show clearer reflectors up to greater depths from the OBN survey; ellipses show important areas where imaging has improved significantly.

3. Methods

In this project, I aim to further characterize the Vlieland Sandstone beyond the relevant background knowledge described in Ch. 1 – 3. I will do this using publicly available data (well-logs) and newly acquired seismic data, which is not yet public. The methodology can be subdivided into three categories:

- data collection and subsequent visualization, enabling decision making for focus areas for the subsequent step;
- characterization of Vlieland Subgroup intervals in well logs, correlating wells and make synthetics for seismic-to-well ties;
- interpretation and surface generation of relevant intervals on seismic, aided by seismic-to-well ties.

From these three steps, the combined findings on thickness distribution of the Vlieland Sandstone Formation and the factors that influence it, will be summarized in a Gross Depositional Environment (GDE) map.

3.1 Data collection

Two main types of subsurface data are used in this project: seismic data and well log data. The program that is usually employed for handling these types of data is SLB's Petrel; it is used by EBN, as well as by the operators that are active in the research area, WINZ (Wintershall Noordzee) and Tenaz. Therefore, the 'working place' for this internship is a Petrel project.

Into the master Petrel-project, data from wells situated in the K15, K18, L13 and L16 blocks are imported (see Fig. 1B). Most wells can be imported from earlier EBN projects on the area, which in turn originally source from openly available data on NLOG (TNO - GDN, 2026a). When data is missing (e.g. earlier studies mention a well-log pattern, but no GR is present in the imported well), it is imported as .LAS file from the NLOG datacenter. 'NLOG well tops' are available for every well in both Excel and in Petrel formats, describing at which MD (measured depth) specific formations and subordinate members can be found. Well tops are checked on their quality, and surfaces that appear outdated or inconsistent with literature are adjusted. The new well tops are processed to create an Excel table, displaying for each well the thickness of the Vlieland Sandstone (KNNS) and Claystone (KNNC), as well as the Holland Formation (KNG), which together sum to the thickness of the Rijnland Group (KN). For each well, the depth of the Base Rijnland Group and the subcropping stratigraphic unit are specified, as well as key information on the availability of specific data. The list of originally imported wells is distilled to list of of key wells. All wells in the key well list 1) have data describing the Vlieland Subgroup interval, being log-data (GR or more) and/or lithological well reports 2) are either exploration or appraisal wells[1]. Development wells are left out to prevent over-representation of locations where hydrocarbon fields were developed. Quality-checked Vlieland Sandstone well-top thickness is compared to the existing GEODE Vlieland Sandstone thickness map. The GEODE map is available on ArcGIS Pro; for better comparison to the analyzed well-tops, the map is recreated in Petrel using the same data and methods as GEODE. This implies interpolation of True Vertical Thickness (dip corrected) values of the Vlieland Sandstone from a selection of wells (see GEODE Metadata (2023)), with cut-off points at TVT = 1 m.

[1] With exception of well K18-KOTTER-08, K18-09 and K18-G-04.

Table 1: Overview of key wells. The columns specify for each well: 1) whether the well is situated within the OBN-area, 2) if the fault is on the side of the hanging wall (basin) or footwall (platform) of the BFB bounding fault, 3) the well name (NLOG), 4) if Gamma-Ray data is available, 4) if a synthetic seismogram is made from this well, 5) if a biostratigraphic report are analyzed for this wel, 6) whether the well is used for any of the well panels (E-W in Fig. 11 & 12, N-S in Fig. 13), 7) with what goal the well was drilled, and the location of the well (8,9).

OBN ?	Structure	Well	GR ?	Seismic-to-well	Biostrat Report	Well Panel	Well Type	Easting	Northing
OBN	Basin	K15-01	Yes		x	E-W, N-S	Exploration	559864	5897755
OBN	Basin	K15-02	Yes	x		E-W	Exploration	566117	5901027
OBN	Basin	K15-03	Yes	x		N-S	Exploration	557589	5904672
OBN	Basin	K15-04B	Yes				Appraisal	558577	5900470
OBN	Basin	K15-07	Yes	x		E-W	Exploration	562912	5899614
OBN	Basin	K15-08	Yes				Appraisal	563754	5902019
OBN	Basin	K15-09	Yes				Exploration	565984	5896641
OBN	Basin	K15-10B	Yes				Appraisal	563424	5902257
OBN	Basin	K15-11	Yes				Appraisal	563778	5902039
	Basin	K15-13	Yes				Exploration	546041	5904304
OBN	Basin	K15-14	Yes				Exploration	553924	5904493
OBN	Basin	K15-15A	Yes				Exploration	563399	5896450
OBN	Basin	K15-FA-106	Yes				Exploration	564941	5900694
OBN	Basin	K15-FA-108	Yes				Exploration	565462	5899685
OBN	Basin	K15-FB-107	Yes				Exploration	558511	5905135
OBN	Basin	K15-FB-108	No				Exploration	558768	5903094
OBN	Basin	K15-FB-109	Yes				Exploration	557531	5904051
	Basin	K15-FC-101	Yes				Exploration	550962	5900780
OBN	Basin	K15-FG-101	Yes	x			Exploration	563153	5906870
OBN	Basin	K15-FG-104	Yes				Exploration	562950	5907170
OBN	Basin	K15-FG-105	Yes				Exploration	563162	5906893
OBN	Basin	K15-FK-101	Yes				Exploration	561506	5896773
OBN	Basin	K15-FK-102A	Yes				Appraisal	561285	5896692
OBN	Basin	K15-FK-103	Yes				Exploration	561186	5897080
OBN	Basin	K15-FK-106	Yes				Exploration	561948	5896866
OBN	Basin	K18-01	Yes		x		Exploration	564814	5881300
OBN	Basin	K18-02-A	Yes		x	N-S	Appraisal	564640	5882459
OBN	Basin	K18-03	Yes	x			Appraisal	565267	5883787
	Basin	K18-04	No				Exploration	552111	5889267
	Basin	K18-05	Yes		x		Exploration	564517	5875410
OBN	Basin	K18-06A	Yes				Exploration	564600	5882068
OBN	Basin	K18-07	Yes				Exploration	565620	5889310
OBN	Platform	K18-09	Yes				Development.	563989	5889376
OBN	Basin	K18-KOTTER-02	Yes				Appraisal	564833	5882636
OBN	Basin	K18-KOTTER-07C	Yes				Exploration	564705	5881962
OBN	Basin	K18-KOTTER-08	Yes	x			Development.	564774	5882308
OBN	Basin	K18-KOTTER-14	Yes		x	N-S	Appraisal	564675	5881962
OBN	Basin	K18-G-04	Yes		x	N-S	Development.	564862	5892087
OBN	Platform	L13-01	Yes				Exploration	569268	5902082
	Platform	L13-02	Yes				Exploration	578562	5903261
OBN	Platform	L13-04	Yes			E-W	Exploration	569852	5898171
OBN	Platform	L13-05	Yes				Exploration	567525	5904550
	Platform	L13-06	No				Exploration	581126	5905660
	Platform	L13-08A	No				Exploration	583169	5907803
	Platform	L13-09	No				Exploration	584666	5899716
	Platform	L13-11	No				Appraisal	584640	5900245
OBN	Platform	L13-13	Yes				Exploration	572943	5899521
	Platform	L13-14	Yes				Exploration	565099	5881339
	Platform	L13-15	Yes				Exploration	578890	5897157
	Platform	L13-16	No				Exploration	585409	5893906
	Platform	L13-17	No				Exploration	586690	5902882
	Platform	L13-FD-101B	No				Exploration	583211	5902353
	Platform	L13-FD-103C	No				Appraisal	584254	5901171
	Platform	L13-FE-101A	No				Exploration	585349	5907730
OBN	Platform	L13-FH-101	Yes	x		E-W	Exploration	573747	5895208
	Basin	L16-01	Yes				Exploration	579598	5881506
	Basin	L16-02	No				Exploration	567384	5879283
	Basin	L16-02A	Yes				Exploration	567384	5879283
OBN	Basin	L16-03	Yes	x		N-S	Appraisal	567976	5879809
	Undef	L16-04	Yes				Exploration	585373	5880186
OBN	Basin	L16-05	Yes	x			Exploration	570220	5880638
	Undef	L16-06	Yes		x		Exploration	581575	5874897
	Undef	L16-07	Yes				Exploration	580532	5875773
	Platform	L16-08	Yes				Exploration	574441	5877231
	Undef	L16-09	Yes				Exploration	583486	5878952
	Undef	L16-10	Yes				Exploration	579596	5876023
	Undef	L16-11	Yes				Exploration	584599	5879856
	Undef	L16-12	Yes				Exploration	579140	5890618

OBN	Platform	L16-14	Yes	x			Exploration	569982	5881356
	Platform	L16-16A	Yes				Exploration	575489	5890187
	Undef	L16-LOGGER-01	No				Appraisal	581989	5874296
	Undef	L16-LOGGER-04A	No				Exploration	581373	5875498
	Undef	L16-LOGGER-09	No				Exploration	581110	5874471
	Undef	L16-LOGGER-10	No				Exploration	582059	5874606
	Undef	L16-LOGGER-10A	No				Exploration	582058	5874600
	Undef	L16-LOGGER-10B	No				Appraisal	581992	5874677

The seismic cube primarily used, is from the newly acquired and recently processed OBN-survey (see Ch. 3.2). This survey determines the research area for this project. The realized time and depth cubes are imported into the project as .ZGY files to avoid high computing times when handling the seismic images. The depth cube was migrated in depth domain; Velocity Model K (see Ch. 3.2) can be used for converting the cube of amplitude data back to the time domain. Two Terracubes, made by Fugro in 2012 by merging multiple 3D surveys, were used. Terracubes 'West' and 'South' are the two relevant cubes for this study; they span a large area in the North Sea, enabling comparison to a larger area for context. On both the Terracubes and the OBN-survey, earlier interpretation work has been done. Interpretations from the DeVli study (2024) done on Terracubes, comprising amongst others Base Vlieland and Top Vlieland, are compared with interpretations done in this project. Interpretations of stratigraphic group boundaries and the major thrust fault, made for construction of Velocity Model K by NAM Offshore B.V., are used for context. Fault interpretations on the OBN-survey from current operators (Tenaz, WINZ) are also imported into the project. Amongst the fault interpretations – apart from numerous faults at Rotliegend level, less relevant for this study – are interpretations from the BFB bounding fault.

3.2 Characterization & Well Correlation

The recreated GEODE thickness map of the Vlieland Sandstone Formation is the starting point for the GDE-map; it provides a plausible 'search area' for Vlieland Sandstones. Analysis and correlation of the GR-log data is the next step for characterizing the Vlieland Subgroup in this area.

Units that subcrop below the Vlieland Subgroup are determined for each well. The subcrop analysis provides context for the depositional setting in terms of fault blocks, with subcrop of younger strata in the basin, and subcrop of older strata on highs/platforms. In addition to the subcrop, the thickness of the Vlieland Claystone is used for indication on paleo-topography. Wells are projected onto seismic lines to gain understanding of the variations in subcrop and stratigraphic unit thickness between wells. The variations in thickness between wells are illustrated in two well panels. A first well panel is constructed perpendicular to the BFB bounding fualt to compare the character of the Vlieland Subgroup on the hanging wall, to its character on the footwall. The second well panel is constructed perpendicular to the paleo-coastline (Jeremiah et al., 2010), in the thickening direction from the Vlieland Sandstone thickness map; this well panel should illustrate the proximal-distal relationship.

Biostratigraphy provides time-surfaces that further illustrate variations in thickness and stratigraphic completeness between wells. For example, a basal transgressive Vlieland unit in one well can have the same age as an interval higher up in the Vlieland Subgroup in the other well. Existing biostratigraphic reports are used; conducting new biostratigraphic analyses is beyond the scope of this project. Part of the biostratigraphic data is adapted from the DeVli study (Bouroullec et al., 2024). Additional data is gathered by inspecting the well datacenter (*Datacenter | NLOG*, 2025) and discussing the found biostratigraphy reports with Roel Verreussel (TNO), an expert on the subject. The resulting biostratigraphic framework is compared to the Wheeler diagrams already available for the Kotter and Helder members (Bouroullec et al., 2024), and used to improve it with more details.

3.3 Seismic interpretation

A further step in improving the resolution of the existing Vlieland Sandstone map, is done by making interpretations of Vlieland Subgroup on seismic. To make reliable interpretations, the seismic character of the Vlieland Subgroup formations, and associated interfaces, is modelled. This is done by generating synthetic seismograms (hereafter: synthetics) from well data and by inspecting seismic volumes.

For a total of 10 wells from the 45 wells in the OBN-survey area, synthetics are created. The wells are selected so that the synthetics capture Vlieland Sandstone at different thicknesses (also at thickness = 0), in different parts of the research area, and with different underburden. Another criterium for the selection of wells is the availability of data: synthetics are created for wells that have density and sonic data available, with exception of the K18-KOTTER-08 well. For this well, a part of the density data is computed using 'Gardner's equation',

$$\rho_b = d\, V_P^f \ ,$$

which is an empirical relationship between rock density ρ_b (g/cm^3) and sonic velocity V_P (µs/ft), using constants f and d (Gardner et al., 1974). The values adapted for the empirical constants are $d = 0.229907$ and $f = 4$, which are Petrel standards that match sedimentary rock empirical relationships (Mavko et al., 2020). Where density/sonic data has gaps, the data is interpolated. Spikes from measuring irregularity are removed with a despiking filter. The synthetics show deterministically how 1D impedance contrasts – calculated from sonic and density – show up on seismic. The synthetics hold information on the type of impedance contrast (positive vs. negative), and the size of the contrast relative to other impedance contrasts in the well (amplitude). Impedance contrasts can indicate a formation top, yet it can also indicate if certain gases or fluids are held. Ricker wavelets of 20 Hz are used for synthetic generation, so not all spikes in calculated impedance contrast show up on the synthetic. Interference of different peaks or troughs is accounted for in calculating the synthetic seismic signal. The synthetics are tied to seismic in time domain, using a wavelet derived from seismic data. Subsequently, Time-Depth Relationships (TDR's) are generated to enable projection of the wells (depth domain) on seismic (time domain). This way, the synthetics provide constraints for interpretation of relevant seismic horizons. Conversely, seismic horizon interpretations reveal more about 2D character of certain intervals on seismic, e.g. whether a surface is characterized by onlaps or truncations.

Seismic interpretation is executed on the time-cube of the OBN-survey, to enhance comparability between seismic volumes and synthetics (generated in TWT). Interpretations on stratigraphic unit scale are available for the OBN-survey, making it possible to directly focus on finding Vlieland Sandstone on seismic. Firstly, the top of the Vlieland Subgroup, is interpreted as 'guiding horizon'. Virtually everywhere in the research area, the top of the Vlieland Subgroup is represented by the interface between the Vlieland Claystone Formation and the Holland Formation (see Fig. 5, Fig. 6). With the homogeneous Vlieland Claystone below it, and the ubiquitous Holland Marl above, the top Vlieland Claystone is expected to be a continuous reflector with a continuous character, as well. The top Vlieland Claystone is interpreted on a grid of inlines and crosslines, adopting an interpretation line increment of 32. Where possible, 3D autotracking was employed, with caution of any lateral changes of seismic character. Next, the Base Vlieland Subgroup and Top Vlieland Sandstone are interpreted, starting from the wells with synthetics available, again in a grid and with 3D autotracking where possible. Several key faults are interpreted as well, to aid interpretation, subsequent surface generation, and illustration of the general geological picture. With faults and horizon interpretations in place, surfaces are generated from relevant horizons. Areas with lower uncertainty are annotated. By subtracting surface depths, vertical thickness of formations is calculated.

4. Results

4.1 Key Wells

An overview of key wells is presented below. Thickness of KN formations were extracted from the TNO well top database (TNO - GDN, 2026) and adjusted where necessary (see Section 3.1). Subcropping units were appended to the table as well, highlighted with colors corresponding to the stratigraphic groups in Fig. 3.

Table 2: Overview of key wells (see also: Table 1) with overview of relevant unit well top thickness (WTT), subcropping unit, and depth of the Vlieland Group in True Vertical Depth (TVD). Data is imported from the NLOG Datacenter (TNO - GDN, 2026a), and quality checked using the GR-log or lithological description of the corresponding well. Abbreviations in columns 4 – 8 correspond to formation codes from DINOloket (TNO - GDN, 2026b). Numbers in the Vlieland Sandstone (KNNS) column are in bold.

OBN?	Structure	Well	KNNC WTT (m)	KNNS WTT (m)	KNN Total WTT (m)	KNG WTT (m)	KN Total WTT (m)	Subcrop	TVD Base KN (m)
OBN	Basin	K15-01	300,9		302,9	94,0	396,9	SLDBN	1528,7
OBN	Basin	K15-02	168,4		168,4	137,0	305,4	RNMUA	2075,2
OBN	Basin	K15-03	205,4		205,4	71,0	276,4	SLDB	1806,6
OBN	Basin	K15-04B	279,5		279,5	115,5	395,0	SLDB	1693,3
OBN	Basin	K15-07	295,7	**4,0**	299,7	113,4	413,1	SLDBC	1944,1
OBN	Basin	K15-08	202,3		202,3	122,5	9,0	SLDB	2296,1
OBN	Basin	K15-09	434,2		434,2	167,4	601,6	SLDB	2069,9
OBN	Basin	K15-10B	217,3		217,3	118,3	335,6	TD	2334,2
OBN	Basin	K15-11	203,2		203,2	90,0	293,1	SLDB	2299,8
	Basin	K15-13	106,0		106,0		106,0	ATWDL	1116,1
OBN	Basin	K15-14	122,0		122,0	45,0	167,0	SLDB	1655,6
OBN	Basin	K15-15A	442,8		442,8	167,2	610,0	SLD	1908,2
OBN	Basin	K15-FA-106	214,3		214,3	135,7	349,9	SLDB	2152,7
OBN	Basin	K15-FA-108	280,4		280,4	137,4	417,8	SLDB	2058,7
OBN	Basin	K15-FB-107	221,0		221,0	206,7	427,8	SLDB	1858,9
OBN	Basin	K15-FB-108	332,4		332,4	100,2	100,2	SLDB	1920,3
OBN	Basin	K15-FB-109	203,6		203,6	69,7	273,3	SLDB	1769,2
	Basin	K15-FC-101	116,0		116,0	43,0	159,0	SLDB	1446,8
OBN	Basin	K15-FG-101	95,0		95,0	99,5	194,5	ATAL	2388,7
OBN	Basin	K15-FG-104	117,1		117,1	73,4	190,4	SLD	2337,9
OBN	Basin	K15-FG-105	114,0		114,0	77,9	191,9	SLD	2367,8
OBN	Basin	K15-FK-101	354,9		354,9	124,3	479,2	SLDBB	1656,1
OBN	Basin	K15-FK-102A	334,2		334,2	118,0	452,2	SLDB	1628,8
OBN	Basin	K15-FK-103	306,9		306,9	109,7	416,5	SLDBB	1579,2
OBN	Basin	K15-FK-106	465,7		465,7	160,3	626,0	SLDB	1803,8
OBN	Basin	K18-01	498,9	**100,0**	598,9	213,0	811,8	SLDBN	1926,6
OBN	Basin	K18-02-A	474,0	**162,4**	636,4	171,0	807,4	SLDBN	1875,3
OBN	Basin	K18-03	390,7	**58,0**	448,6	173,4	622,0	SLDBN	1823,0
	Basin	K18-04	595,1		595,1	7,0	602,1	ZE	1975,6
	Basin	K18-05	811,1	**245,8**	1056,8		1056,8	SLDBN	2116,3
OBN	Basin	K18-06A	452,8	**142,6**	595,4	203,6	798,9	SLDBN	1850,9
OBN	Basin	K18-07	92,0		92,0		92,0	SLDB	1208,8
OBN	Platform	K18-09		**45,0**	45,0		45,0	DC	3325,0
OBN	Basin	K18-KOTTER-02	476,1	**166,6**	642,7	184,9	827,6	SLDB	1886,5
OBN	Basin	K18-KOTTER-07C	436,5	**142,5**	579,0	154,4	733,4	SLDBN	1844,6
OBN	Basin	K18-KOTTER-08	459,6	**162,9**	622,5	184,9	807,4	SLDBN	1871,8
OBN	Basin	K18-KOTTER-14	447,9	**138,8**	586,8	182,1	768,8	SLDBN	1864,7
OBN	Basin	K18-G-04	307,4	**38,6**	346,0		346,0	SLDB	1447,5
OBN	Platform	L13-01	193,6		193,6	156,0	349,6	RB	2590,3
	Platform	L13-02	170,2	**23,3**	193,5	112,1	305,6	RBSHM	2946,9
OBN	Platform	L13-04	218,7		218,7	149,8	368,6	ZE	3136,7
OBN	Platform	L13-05	47,0		47,0	103,5	150,5	RBMDC	1775,5
	Platform	L13-06	217,9		217,9	172,9	390,8	RB	2962,8
	Platform	L13-08A	207,7		207,7	171,4	379,2	RB	3228,4
	Platform	L13-09	166,6	**21,5**	188,1	165,6	353,7	RBSM	3170,1
	Platform	L13-11	170,3	**3,4**	173,7	239,9	413,6	RBSM	3148,5
OBN	Platform	L13-13	130,0		130,0	158,1	288,1	RBSHM	2364,5
	Platform	L13-14	176,9		176,9	154,5	331,4	RBSHM	2779,8
	Platform	L13-15	123,0	**7,0**	130,0	170,0	300,0	ZE	3289,6
	Platform	L13-16	131,0		131,0	183,0	314,0	ZE	3227,4
	Platform	L13-17	134,0		134,0	181,8	315,8	ZE	3203,3
	Platform	L13-FD-101B	207,5	**5,0**	212,4	185,9	398,3	RBSM	3109,4
	Platform	L13-FD-103C	222,4		222,4	169,3	391,7	RB	3135,7
	Platform	L13-FE-101A	143,5		143,5	200,1	343,7	ZE	3256,3
OBN	Platform	L13-FH-101	204,8	**24,0**	228,8	201,0	429,7	RBSHM	2965,9
	Basin	L16-01	177,5	**3,0**	180,5	262,3	442,8	RBSM	2730,3
	Basin	L16-02	251,0	**37,4**	288,5	172,3	460,8	SLDB	2087,9
	Basin	L16-02A	251,0	**37,4**	288,5	172,3	460,8	SLDB	2087,9

OBN	Basin	L16-03	242,6	**30,0**	272,6	180,7	453,3	SLDB	1920,1
	Undef	L16-04	124,0	**25,5**	149,5	221,0	370,4	RB	2871,9
OBN	Basin	L16-05	70,0	**16,0**	86,0		86,0	SLDB	1052,4
	Undef	L16-06	274,8	**17,0**	291,8	353,4	645,3	ATAL	2493,6
	Undef	L16-07	182,7	**10,0**	192,7	337,9	530,6	ATAL	2011,1
	Platform	L16-08	379,8	**29,2**	409,0	192,6	601,6	SLDB	2987,4
	Undef	L16-09	142,8	**44,0**	186,8	224,8	411,6	RBSM	2432,7
	Undef	L16-10	503,8	**17,8**	521,6	469,6	991,2	ATAL	2859,7
	Undef	L16-11	166,7	**16,0**	182,7	271,4	454,0	RBSM	2893,6
	Undef	L16-12	132,4	**1,0**	133,4	213,8	347,2	ZE	3201,7
OBN	Platform	L16-14	116,9	**12,0**	128,9	98,5	227,4	ZE	3121,7
	Platform	L16-16A	242,5		242,5	207,8	450,4	RBSH	3147,1
	Undef	L16-LOGGER-01	154,0	**27,0**	180,9	186,3	367,2	ATAL	1932,3
	Undef	L16-LOGGER-04A	274,1	**59,3**	333,4	526,3	859,8	ATAL	2855,6
	Undef	L16-LOGGER-09	147,9	**10,9**	158,8	346,1	504,9	RNRO	2085,3
	Undef	L16-LOGGER-10	362,9	**13,9**	376,8	349,7	726,5	TD	2181,7
	Undef	L16-LOGGER-10A	532,0	**67,7**	599,8	549,9	1149,7	RBSM	2604,9
	Undef	L16-LOGGER-10B	227,1	**41,0**	268,1	87,6	355,7	TD	2041,4

The quality-checked well thickness (Table 2) is compared to replication of the regional GEODE Sandstone thickness map (Fig. 9). This regional map was made for the Lower Cretaceous GEODE Chapter (Ten Veen et al., 2023), by interpolating well thickness and combining that with erosional surfaces of the DGM-Model (Fig. 9). A sharp increase in Vlieland Sandstone thickness provides an indication for the position of the NNW-SSE basin bounding fault. This thickness increase is less steep in the OBN-survey area, especially in the north. Within the OBN-area, the thickest KNNS well intervals are in the Kotter field area, KNNS thickness decreases away from the field. The Vlieland Sandstone well top thickness (from Table 2) was plotted as colored circles on top of the GEODE thickness map. The color discrepancies between circles and contour map indicate that the thickness contouring is not honoring the thicknesses observed at all the wells. Close to faults, for example, discrepancies are in line with expectation: wells with a fault in the Vlieland Sandstone Formation interval, were not used for GEODE thickness interpolation (J. H. Ten Veen et al., 2023). Another thing that stands out is the 'bulls-eye' of high thickness values on the map, close to the Kotter field. Presumably, this bulge is not present in the thickness of the Vlieland Sandstone itself. Rather, it is an artefact of the interpolation method in combination with the closely spaced data points with high difference in thickness values. Discrepancies between well thickness and map thickness, and the bulls-eye geometry, are both agreeable for a regional map: the dataset for the GEODE maps is large and meant to be used for regional purposes. In a regional map, thicknesses from wells with faults would presumably result in thickness anomalies with point-like geometry. For this local study however, information from each well with a Vlieland Subgroup interval was used.

(Next page) Figure 9: Vlieland Sandstone thickness map from GEODE (Ten Veen et al., 2023). Colored circles are Vlieland Sandstone thickness at wells from this study (Table 2). OBN-survey area is denoted as a black polygon. Oil- and gas fields at Rijnland level are depicted in white polygons. Grey diamonds denote wells with zero Vlieland Sandstone in Table 2. Deviations in thickness between the map and the well data are variable across the study area, but no more than 35m. Contour interval figure 9A = 10m, contour interval figure 9B = 5 m.

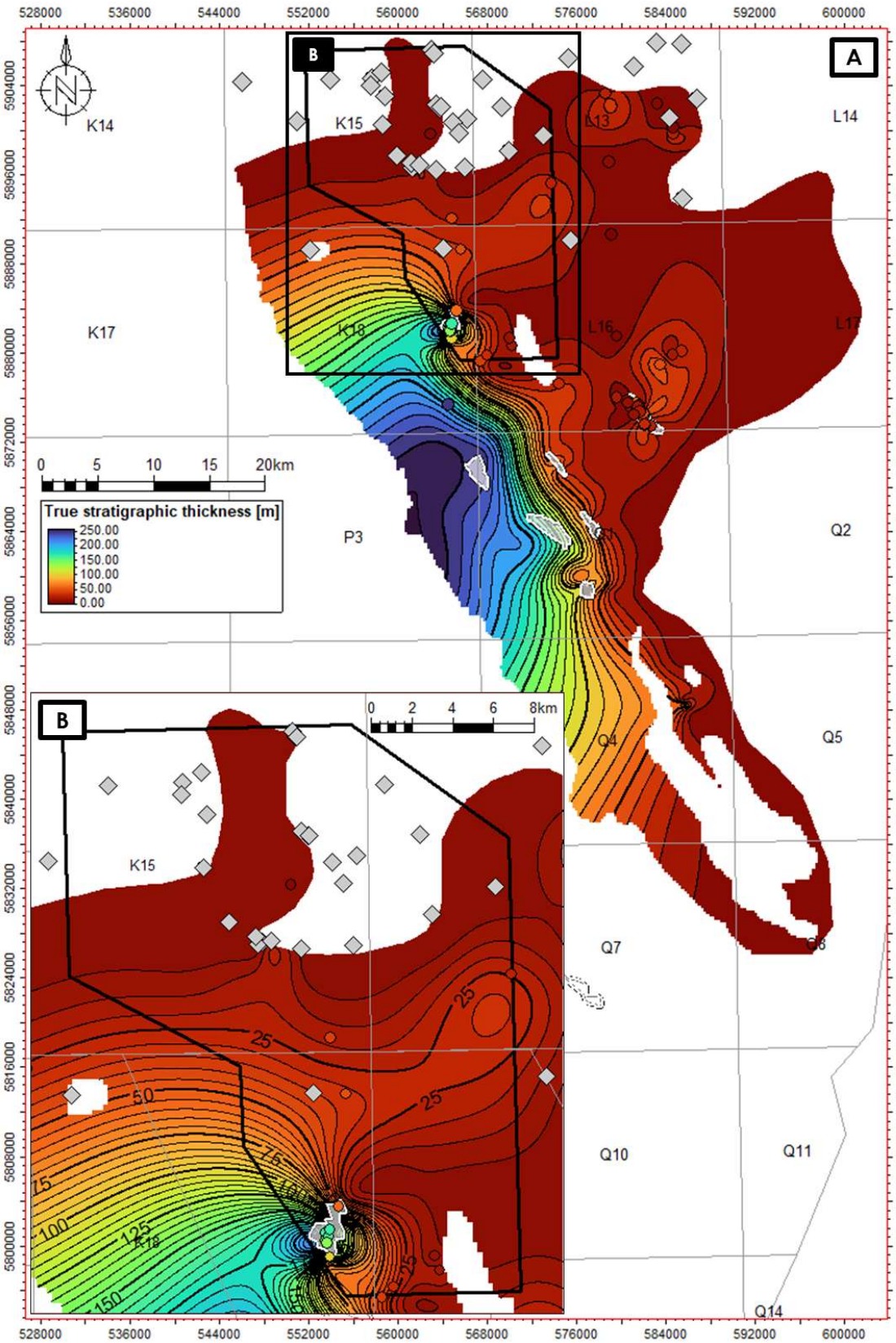
A
B
B
K14
K15
K17
K18
L13
L14
L16
P3
Q2
Q4
Q5
Q7
Q10
Q11
Q14
0 5 10 15 20km
True stratigraphic thickness [m]
250.00
200.00
150.00
100.00
50.00
0.00
0 2 4 6 8km
528000 536000 544000 552000 560000 568000 576000 584000 592000 600000
5904000 5896000 5888000 5880000 5872000 5864000 5856000 5848000 5840000 5832000 5824000 5816000 5808000 5800000

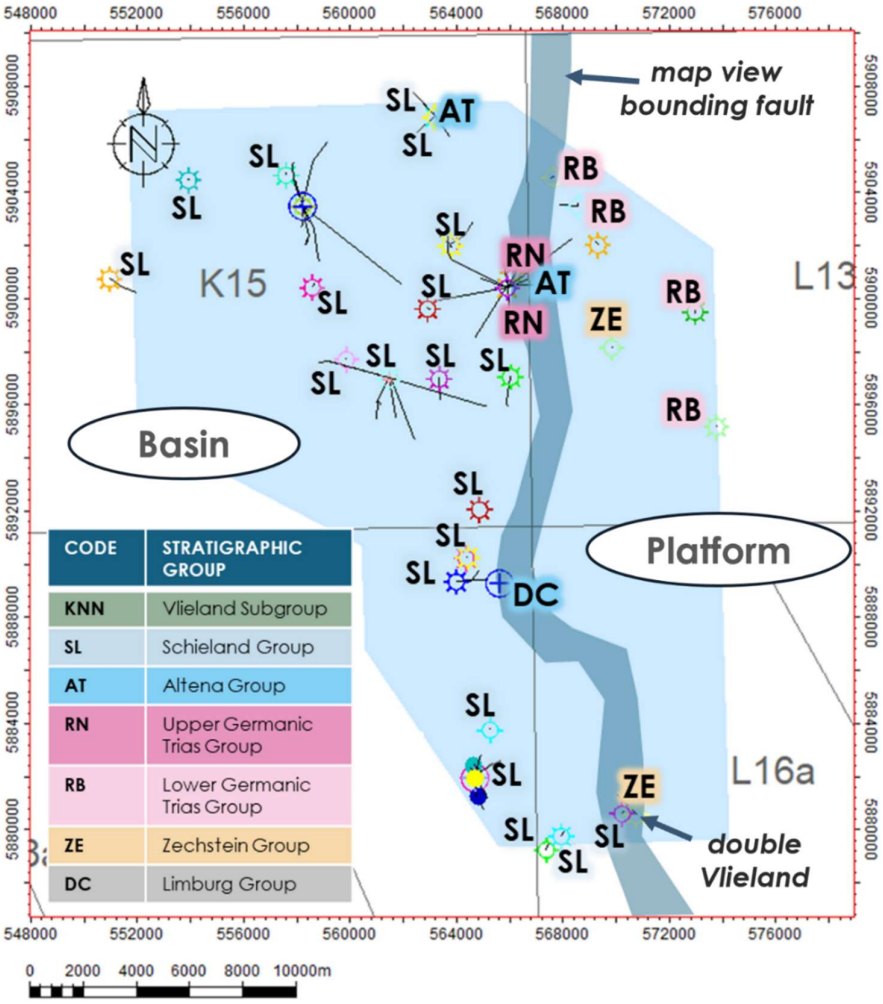

Figure 10: Subcrops in wells in the OBN-area. Each well head (or group of well heads) is labeled with the subcropping stratigraphic unit, with shadow in corresponding color. OBN-survey area is shaded in light blue, the approximate position of the basin bounding fault is shaded in dark grey. The Schieland Group subcrops below the Vlieland Subgroup west of the BFB bounding fault, older units subcrop west the bounding fault.

The stratigraphic units that subcrop below the Vlieland Subgroup (see Table1) within the OBN-survey area, are displayed in map view in Figure 10. In wells west of the fault zone, almost everywhere the Schieland (SL) is found below the Vlieland Subgroup, while in wells to the east units of Lower Triassic (RB) and older age are found below the Vlieland Subgroup.

4.2 Well Panels

In two well panels (Figs. 11 and 12), the distribution of stratigraphic units from west to east, perpendicular to the main bounding fault of the BFB, is visualised. The two panels display the exact same wells, yet the panels are flattened to different stratigraphic levels. The first panel shows how the main bounding fault influences the distribution of syn-tectonic sediments. The second panel illustrates the implications of reverse reactivation of the main bounding fault.

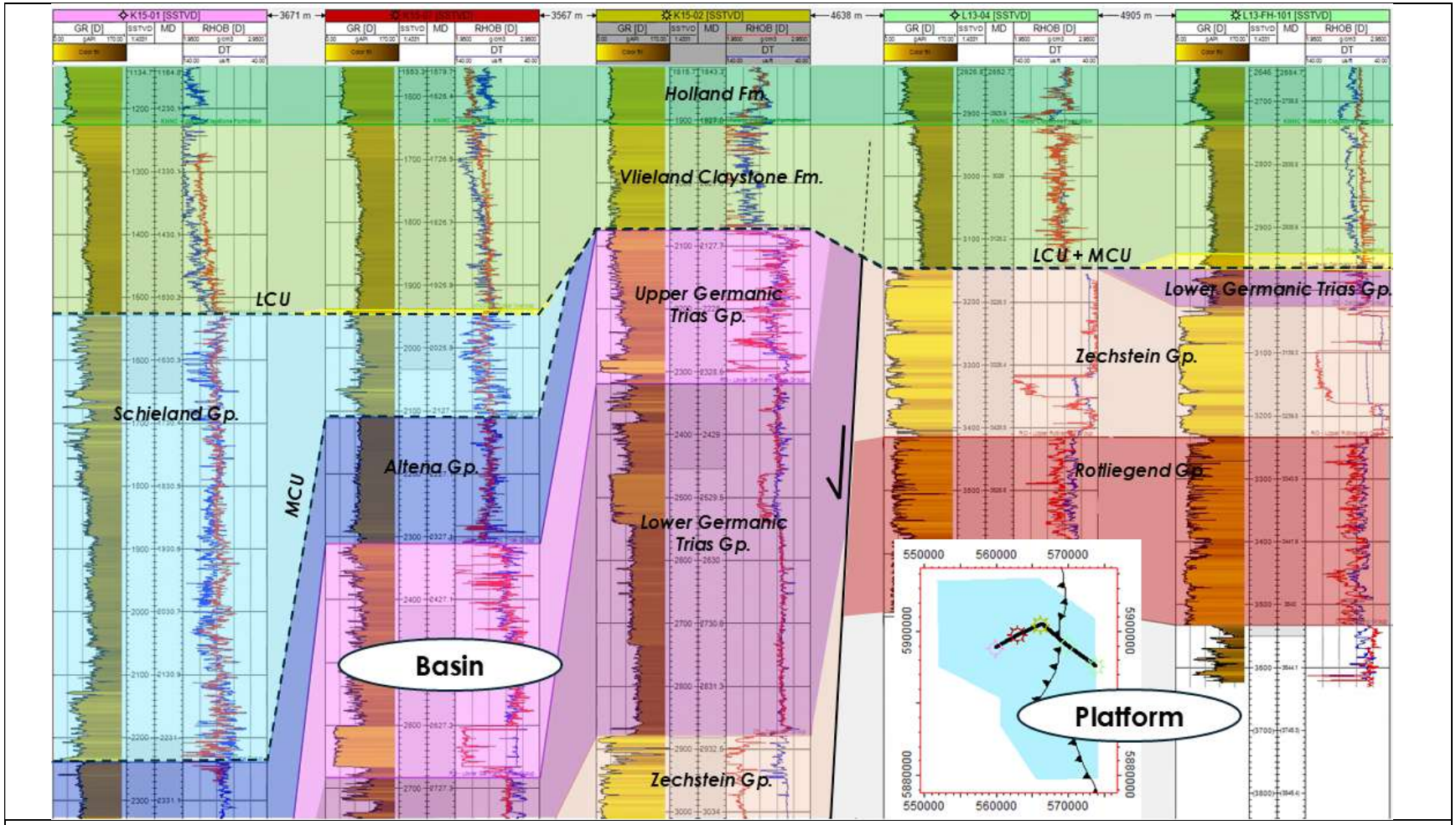

Figure 11: Well panel from west to east in the northern part of the research area, across the main bounding fault of the Broad Fourteens Basin (inset figure). Wells included are (from east to west): K15-01, K15-07, K15-02, L13-04, L13-FH-101. Correlations between wells are supported by seismic data between wells. The section is flattened to the Top Vlieland Claystone Formation for visualization of the BFB and bordering platform during deposition of the final transgressive units. In the basin, Triassic and Jurassic units are present, while on the platform, these units are absent or relatively thin. The thickest Kotter interval in this well section is 24 m. MCU= Mid Cimmerian Unconformity, LCU = Late Cimmerian Unconformity (see Fig. 3).

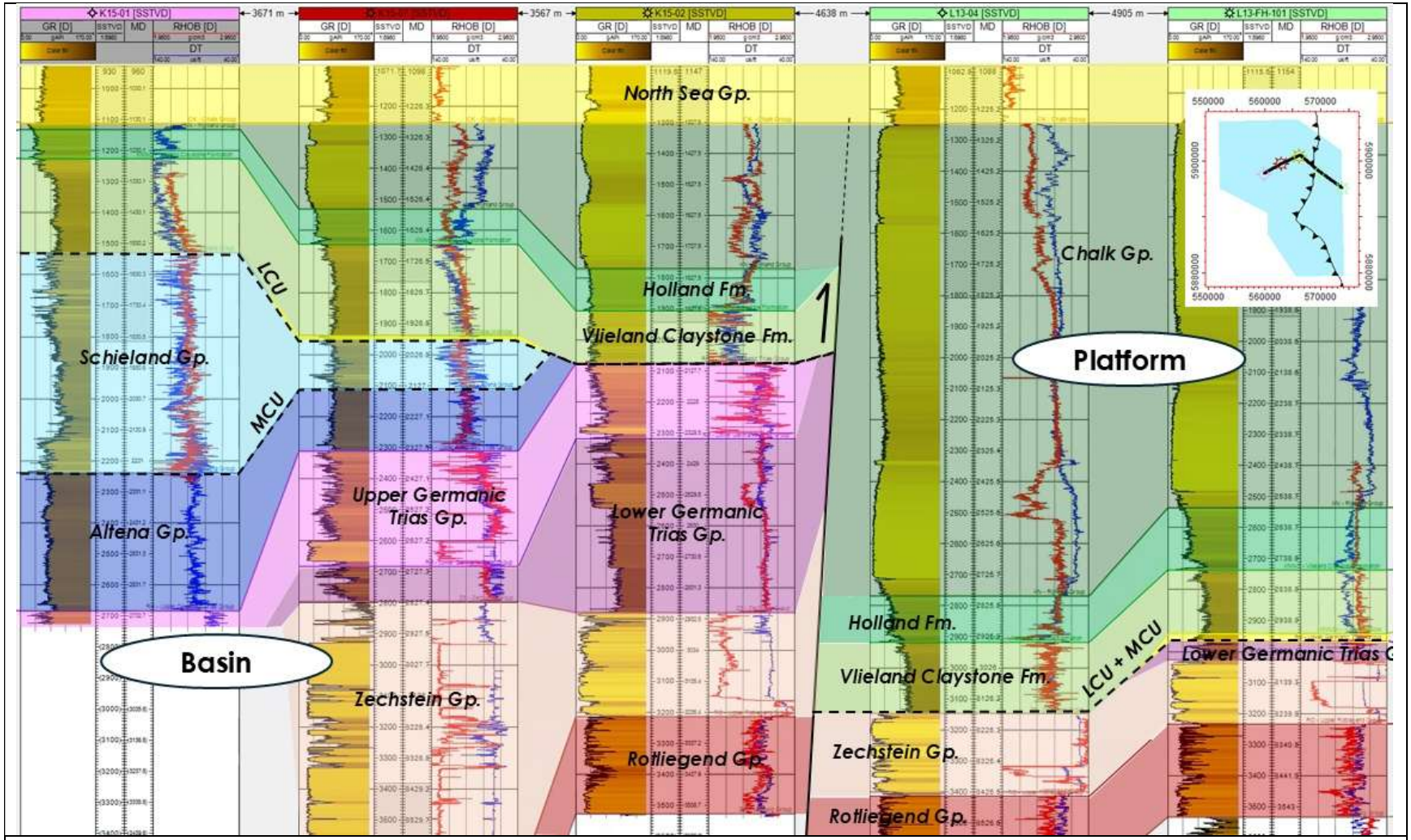

Figure 12: Well panel from west to east, displaying the same wells as Figure 11, in the same order. Correlations between wells are again supported by seismic data between wells. This panel is flattened to the Top Chalk Group, here i.e. Base North Sea Group, to illustrate the differential accommodation for the Chalk Group due to reverse reactivation of the BFB main bounding fault. Abbreviations are explained in the caption of Figure 11.

By comparing the two panels, the influence of Cimmerian rifting (Fig. 11) and subsequent Alpine inversion (Fig. 12) becomes apparent. The depocenter of the Altena and Schieland Groups is west of the bounding fault, while the Chalk depocenter is in the east. The grouped Cimmerian unconformities cut deep into the stratigraphy of the platform. The absence of Upper Triassic and Jurassic stratigraphic groups can be attributed to non-deposition, erosion, or a combination of the two. Which factor contributed the most, is not apparent from the well panels. The panels comprise wells in the northern part of the research area, where the thickness of the Vlieland Sandstone Formation is limited; the thickest sandstones are deposited in the southern part of the OBN area, West of the BFB bounding fault (Fig. 9).

The Vlieland Sandstone Formation thickens towards the south, in accordance with the rapid SW-directed transgression described by Jeremiah et al. (2010). In well L16-03, at the southernmost part of the OBN-survey area, the Vlieland Sandstone thickness decreases again, just like the Vlieland Claystone in this well. The Vlieland Sandstone Formation depositional environment is interpreted as marine, and upper shoreface (Bouroullec et al., 2024; Jeremiah et al., 2010; see Ch. 2.1.2). Within the sandy intervals of the three southernmost wells, a short high-GR interval was observed. In a core description of K18-02-A, this interval is attributed to a lagoonal depositional setting (Bouroullec et al., 2024). For the well correlation panel, it was assumed that the intra-sand high-GR interval of well L16-03 can be attributed to the same depositional setting. Between the lowest-GR sandstone and Vlieland Claystone, several meters of intermediate GR were seen in well K18-02-A and well L16-03. Jeremiah et al. (2010) acknowledged this interval in K18-02-A and interpreted it as lower shoreface sandstones. In more wells, including well L16-03, this intermediate GR interval was observed (Fig. 13) and assumed to have lower shoreface depositional setting based on correlation. West of the bounding fault, so within the BFB basin, the variations well top thickness were analyzed on Vlieland Subgroup level (Fig. 13).

The wells in the panel in Fig. 13 lack any additional obvious intra-Vlieland similarities: biostratigraphic data was considered to strengthen the correlation between wells. For all wells except K15-03, the lowermost Vlieland had biostratigraphic reports available. This enables comparison of chronostratigraphy between wells. Within the fluvial to lagoonal Schieland Group, biostratigraphic data is sparse and/or unreliable (Bouroullec et al., 2024). The lowermost interval with marine fossils available, corresponding to the marine Vlieland Subgroup by definition, is dated in all wells of Figure 13, except well K15-03. The lowermost Vlieland Subgroup in all these wells is dated to Latest Ryazanian / Early (or Earliest) Valanginian (red arrows); irrespective of this dated interval being Vlieland Sandstone or Vlieland Claystone Formation. This is again in accordance with the SE-directed transgression (see Ch 2.1.2): while deep marine claystones were deposited at the location of well K15-01, a shallow marine environment prevailed in the southeast. As the lowermost Vlieland has the same age in all dated wells, it is likely that this is also the case for other wells in the basin, like well K15-03. Wells K15-01, K18-KOTTER-14 and L16-03, have intervals dated as Valanginian – Early Hauterivian (Fig. 13, orange arrows). In wells K15-01 and L16-03, the Valanginian – Early Hauterivian interval is in the Vlieland Claystone Formation, in well K18-KOTTER-14 the Vlieland Sandstone Formation has this age. This suggests that accommodation space or sediment supply of sand remained longer at the location of this well. Two wells have an interval dated as Barremian (Fig. 13, yellow arrows). Therefore, it is likely that the stratigraphy in these wells is relatively complete. Since the other wells also contain a large claystone interval, assumably the stratigraphic record is relatively complete in all wells.

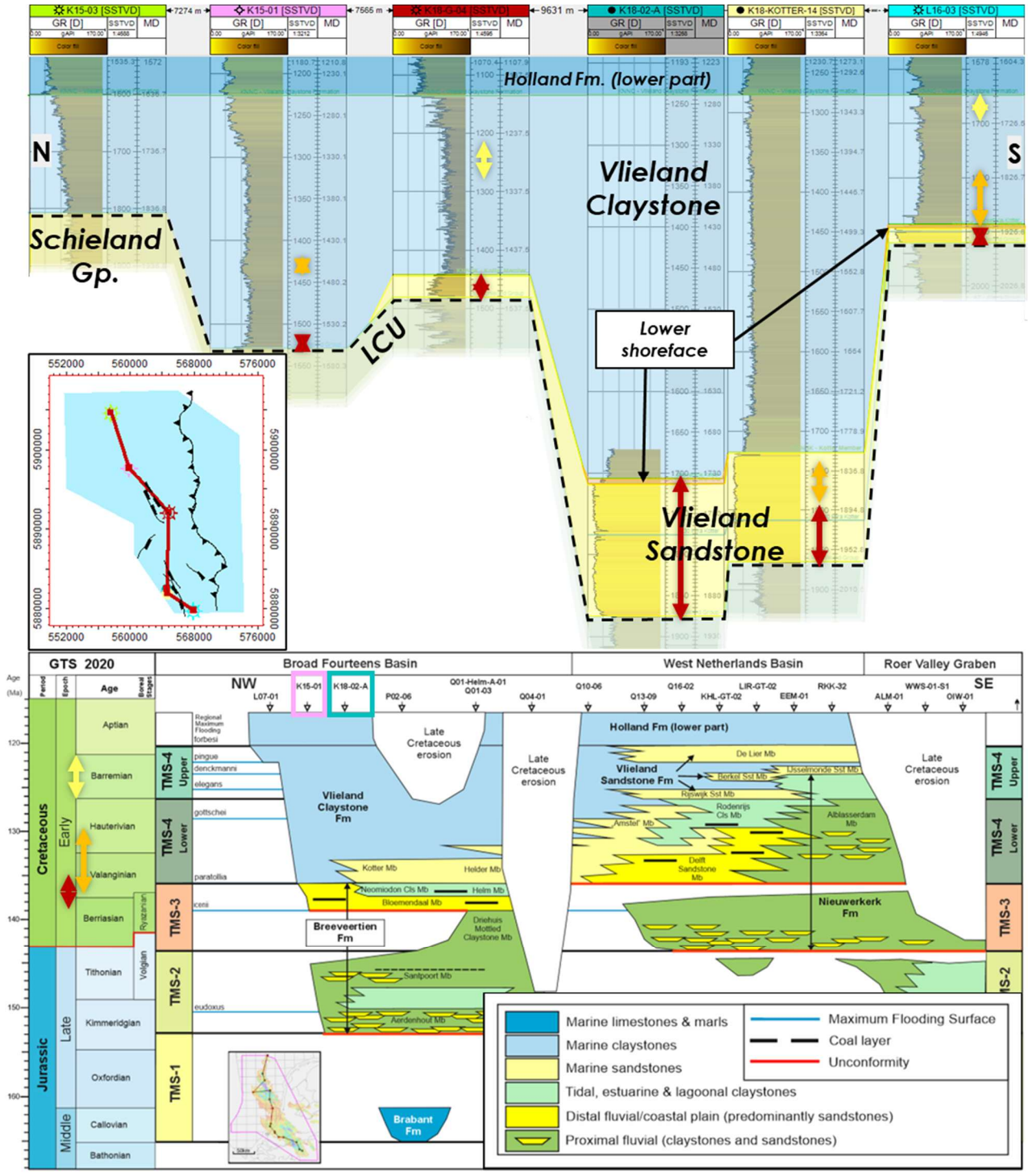

Figure 13: (top figure) Well panel from northwest to southeast, west of the BFB bounding fault, flattened to Top Vlieland Claystone. Context for the location is given on the map view of the panel, together with map view of interpreted faults. (bottom figure) Context for depositional environment is given on the Wheeler diagram, adapted from TNO (Bouroullec et al., 2024). Well K15-01 and K18-02-A (pink & turquoise) appear both in the well panel and in the wheeler diagram. Intervals dated with marine biostratigraphic data are indicated with double arrows in the SSTVD column from the well panel. Corresponding colors are used for the chronostratigraphic intervals indicated next to the Wheeler diagram. Biostratigraphic information is adapted from the DeVli report (Bouroullec et al., 2024) and from reports available on the NLOG Datacenter (TNO - GDN, 2026a), from TNO (Munsterman et al., 2012) and Robertson Research International (Haskins et al., 1978).

4.3 Synthetic Seismograms

Synthetics were created for 10 wells in total (see Table 1). An overview of the results is presented in Table 3 and examples of synthetics are shown in the figures that follow. In each figure with seismic data, the seismic convention of EBN is adopted (Fig. 14).

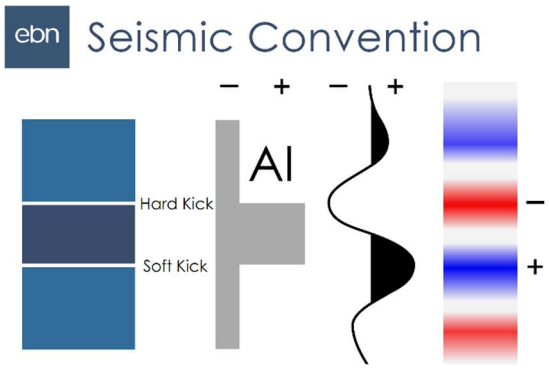

Figure 14: EBN seismic convention. Positive Acoustic Impedance (AI) contrasts displayed as a trough and/or in red. Negative AI contrasts are denoted as a peak and/or in blue.

The table below specifies the seismic characteristics of interfaces in wells, that followed from synthetic generation and seismic-to-well ties.

Table 3: Overview of seismic characterization results. For each well is specified: the presence and depth extent of density- and sonic data, the unit subcropping below the Vlieland, the Vlieland Sandstone well top thickness (SSTVD, after quality check), and the character of the seismic reflections (i.e. change in acoustic impedance) at the three surfaces for interpretation (Top Vieland Claystone, Top Vlieland Sandstone and Base Vlieland Subgroup). [1]Missing sections of the density log are calculated with sonic, using Gardner's equation (see Section 3.3); [2]All density data is calculated using Gardner's equation; B.R. = appears Below Resolution.

Well	Presence DT & DEN	Subcrop	KNNS TTW (m)	Top KNNC	Top KNNS	Base KN
K15-02	Both, mid CK → RO	RNMUA	x	Thick soft kick	N/A	KNNC to SL: cutoff SL reflectors
K15-03	Both, N → RO	SLDB	x	Thick soft kick	N/A	KNNC to SL: cutoff SL reflectors
K15-07	Both, N → ZE	SLDB	4m	Lowest hard kick of hard – soft - hard	B.R. (or zero crossing hard to soft?)	KNNC to SL: broad soft kick
K15-FG-101	DT: N → RO DEN: RO	SLDBN	12m	Soft kick	B.R. (or zero crossing?)	KN to SL: hard kick?
K18-03	Both, mid KNNC → SL	SLDBN	55m	N/A	Vague hard kick?	KNNS to SL: soft kick
K18-KOTTER-08	DT: mid CK → SL DEN: mid KNNC → SL[1]	SLDBN	155m	N/A	Soft kick	KNNS to SL: soft kick
L13-FH-101	Both, N → ZE	RBSHM	12m	Thick soft kick	Zero crossing hard to soft?	KN to RB: soft kick?
L16-03	Both, N → ZE	SLDB	30m	Lowest hard kick of hard – soft - hard	Hard kick?	KNNS to SL: soft kick
L16-05	Both, mid KNNC → ZE	SLDB	8m	Hard kick (below NS group)	B.R. (or zero crossing hard to soft?)	KN to SL: soft kick
L16-14	DT: N → ZE DEN [2]	ZE	16m	Soft kick (?)	B.R. (or zero crossing hard to soft?)	KN to SL: soft kick

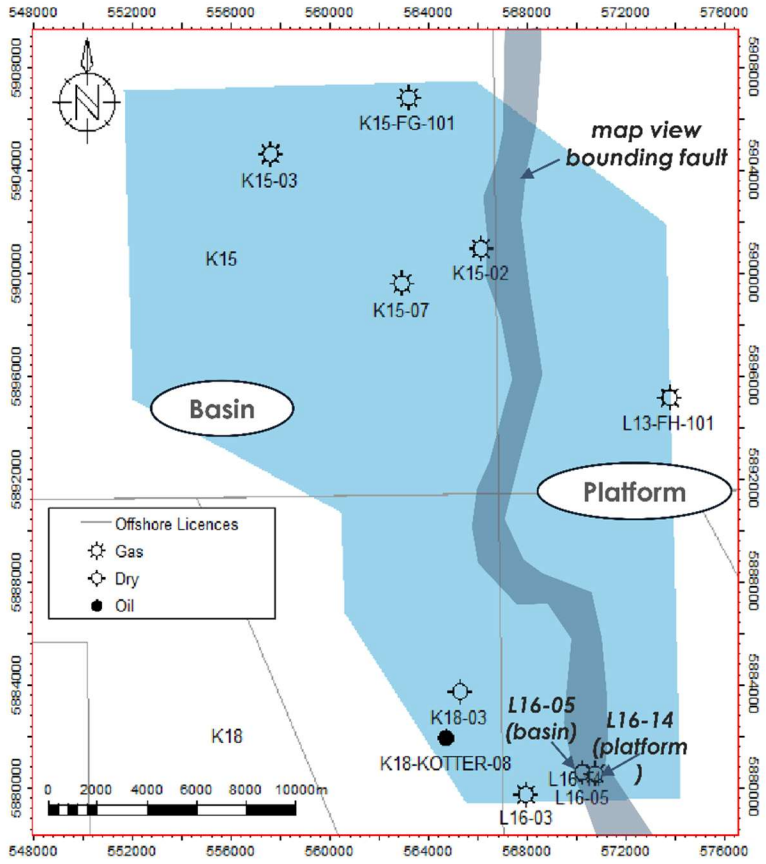

The selected wells all have sonic and density data over the depth range of interest, except wells K18-KOTTER-08 and L16-14. For these wells, density logs were (partly) calculated from sonic (see Section 3.3). Wells were selected to encapsulate a wide range of Vlieland Sandstone thicknesses (including zero thickness), as well as a variety of subcropping units. Furthermore, locations of selected wells were aimed to be distributed evenly over the OBN-area, covering both the platform and the basin.

Figure 15: Wells used for synthetic generation. Learnings per well are described in Table 3.

In and around the Kotter field, the highest well-top thicknesses of the Kotter Member were expected (see Fig. 9), and hence visibility on seismic. For one of the Kotter field wells, K18-KOTTER-08, a synthetic seismogram was calculated. The synthetic seismogram has a good tie to the seismic cube in TWT (see Fig. 16). An overview of synthetic generation and subsequent seismic characterization of interfaces is presented in Figure 16.

Note that the Top Vlieland Claystone is not picked on the soft kick expected for the transition from harder marls to softer clays. Rather, it is picked on the hard kick above, which is the lowest hard kick in a hard – soft – hard triplet as indicated on the 2D cross-section. This triplet is related to impedance contrasts from the lowermost Holland Formation members and is more easily traceable than to the soft kick below it. The triplet can be related to the GR-pattern, showing a transition to clay and then back to marl, accounting for the positive and then negative impedance contrast.

Both the Top Vlieland Sandstone (KNNS) and the Base Vlieland Subgoup (KNN) (or Base Rijnland Group (KN)) are picked on a clear soft kick in this well, with relatively high amplitude compared to surrounding peaks and troughs. The Base KN soft kick can be explained by the softer Neomidon Claystone below KNNS here. The Top KNNS soft kick could be explained by the occurrence of hydrocarbons in the Kotter field. This hypothesis was tested by comparing to a nearby well with sandstone thickness above expected resolution, but with no hydrocarbon shows in KNNS.

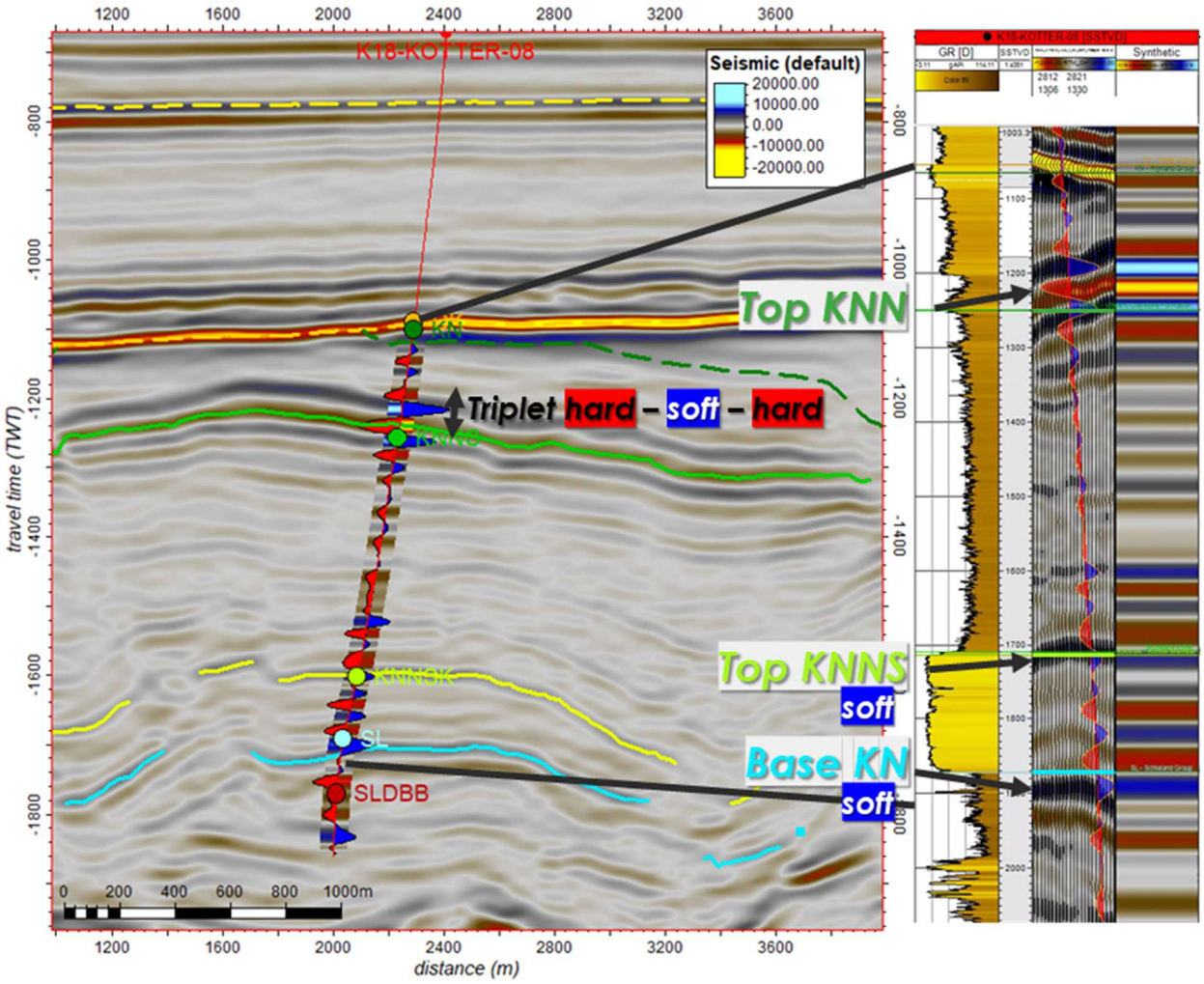

Figure 16: Seismic-to-well tie for well K18-KOTTER-08. The synthetic was calculated using density and sonic logs and tied to seismic in TWT. On the left, the synthetic is displayed in a single wiggle, on a bitmap with corresponding colors, on a cross-section of the TWT cube along the well trajectory. Dashed lines represent earlier interpretations on this same cube; in this figure the Base North Sea and Base Upper North Sea are interpreted. On the right, the well logs displayed are: GR, time OBN-seismic along the well with synthetic along the trajectory, and synthetic as a bitmap log.

In well K18-03, the top of the Kotter member does not display the same clear soft kick in the synthetic nor on seismic (Fig. 17). Rather, a vague hard kick appeared to represent the transition from Vlieland Claystone to Vlieland Sandstone in well K18-03. Oil was found in the Kotter interval of the K18-KOTTER-08 well (see Fig. 16, oil), while the same Kotter interval was found to be water-bearing (see Fig. 17, dry). This supports the hypothesis that the seismic character of Top Vlieland Sandstone is influenced by hydrocarbon presence. However, a difference in porosity (governed by lower pressures due to hydrocarbon absence) or other differences in sandstone facies (clay content, cement) could also influence the impedance contrast. Given the variable seismic character, the offset of Top and Base Vlieland Sandstone horizons on faults could not be well constrained. With increasing depth, the fault geometry (reverse/normal) appears to change (see Fig. 17), adding to uncertainty of horizon interpretation even more.

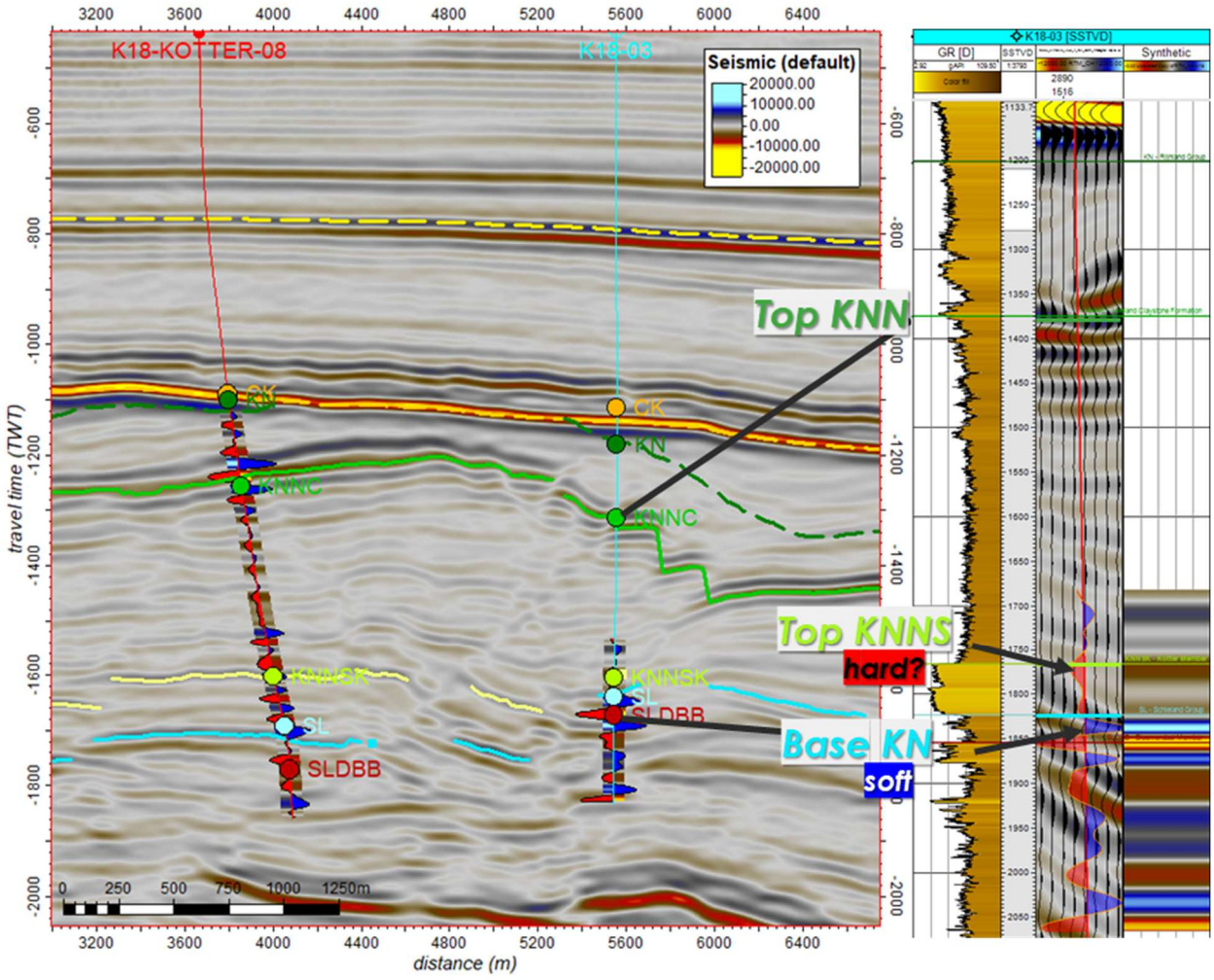

Figure 17: Seismic-to-well tie for well K18-03. The synthetic was calculated using density and sonic logs and tied to seismic in TWT. On the left, the synthetics are displayed as with wiggles, on a bitmap with corresponding colors, on a cross-section of the TWT connecting the well heads of K18-KOTTER-08 and K18-03 (see Fig. 15). Dashed lines represent earlier interpretations on this same cube; in this figure again the Base North Sea and Base Upper North Sea are interpreted. On the right, the well logs displayed are: GR, time OBN-seismic along the well with synthetic along the trajectory, and synthetic as a bitmap log.

The same applied when attempting continuous horizon interpretation from the latter K18 wells to well L16-03. At well L16-03, the Vlieland Sandstone Formation is even thinner (see Table 3). The Base Vlieland Subgroup was assumed to be a soft kick here (Fig. 18); Top Vlieland Sandstone was picked in context of the Base Vlieland Subgroup, which was picked on a soft kick in this well. The Top Vlieland Sandstone was picked on the next S-crossing above. The Top Vlieland Claystone was again picked on the lowest hard kick in a hard – soft – hard triplet, like in well K18-KOTTER-08 (Fig. 16).

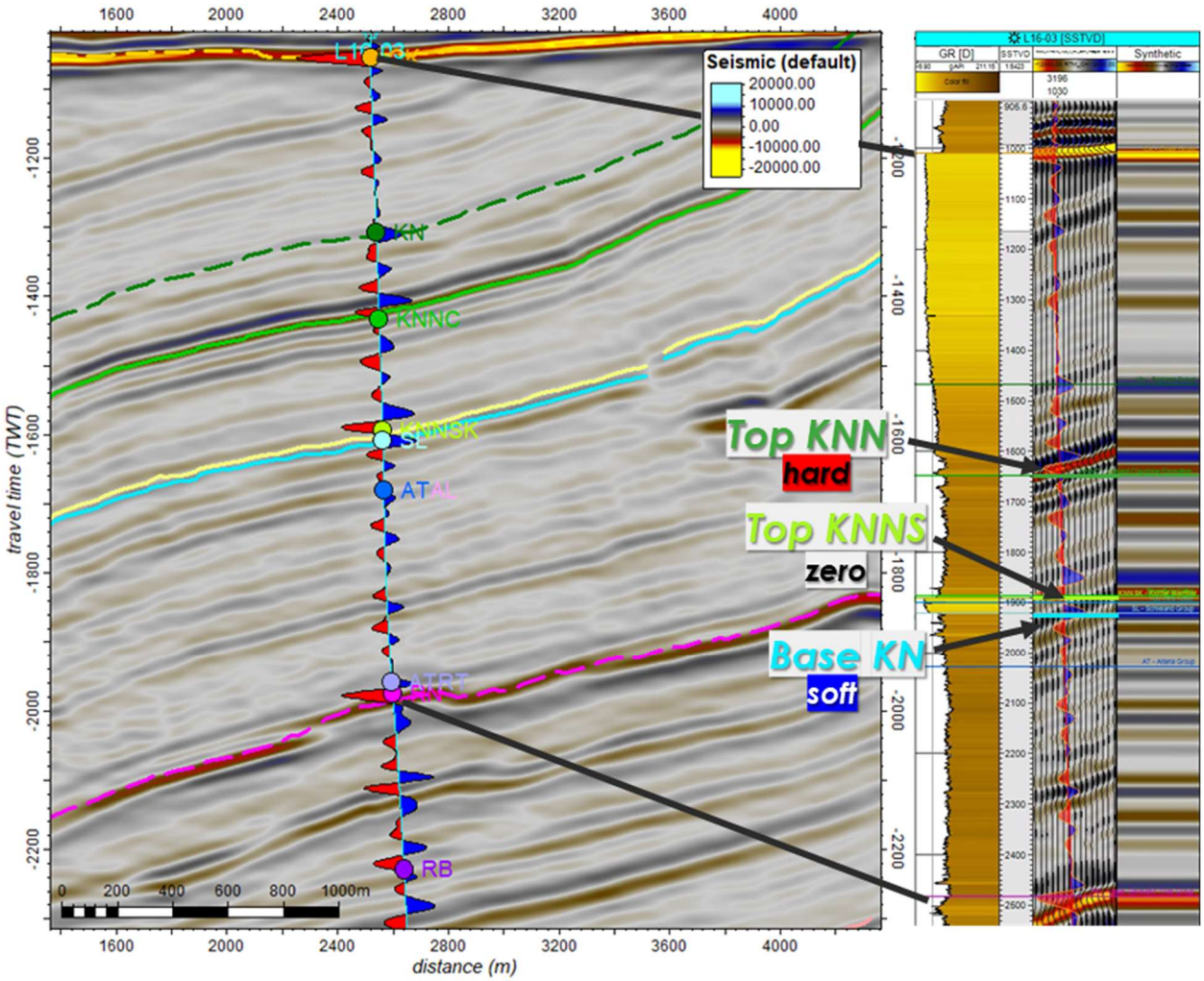

Figure 18: Seismic-to-well tie for well L16-03. The synthetic was calculated using density and sonic logs and tied to seismic in TWT. On the left, the synthetic is displayed in a single wiggle, on a bitmap with corresponding colors, on a cross-section of the TWT cube along the well trajectory. Dashed lines represent earlier interpretations on this same cube; in this figure the Top Upper Triassic, Base Chalk, and Base North Sea are interpreted. On the right, the well logs displayed are: GR, time OBN-seismic along the well with synthetic along the trajectory, and synthetic as a bitmap log.

The seismic character of the Base Vlieland Subgroup changes towards the north of the research area. In the aforementioned wells, the Schieland Group reflectors were parallel to the Vlieland Subgroup reflectors. In well K15-03 however, an angular unconformity is clearly visible as the Base Vlieland Subgroup: Schieland Group reflectors terminate at an angle to the Vlieland Subgroup reflectors (Fig. 19). The unconformable contact inhibited following one type of amplitude for the Base Vlieland Subgroup: different lithologies subcrop below, hence the impedance contrasts varied laterally. Therefore, in the area where Schieland Group reflectors were not parallel to those of the Vlieland Subgroup, the Base Vlieland Subgroup was picked at reflector terminations. At faults, lining up terminations was more difficult; uncertainty of horizon depth was higher here.

The character of the Top Vlieland Claystone is also different in the north. The synthetic of well K15-03 demonstrates why a soft kick was picked for the top Vlieland Claystone rather than the hard – soft – hard triplet (Fig. 19). On seismic, it was observed that the transition between the two different characters is gradual; the hard kick picked for the Top Vlieland Claystone in the south slowly dies out into the soft kicks above and below

towards the north. This change in character can be attributed to a decrease in Holland member thickness: the impedance contrast from the lowest Marl member goes below resolution at well K15-03.

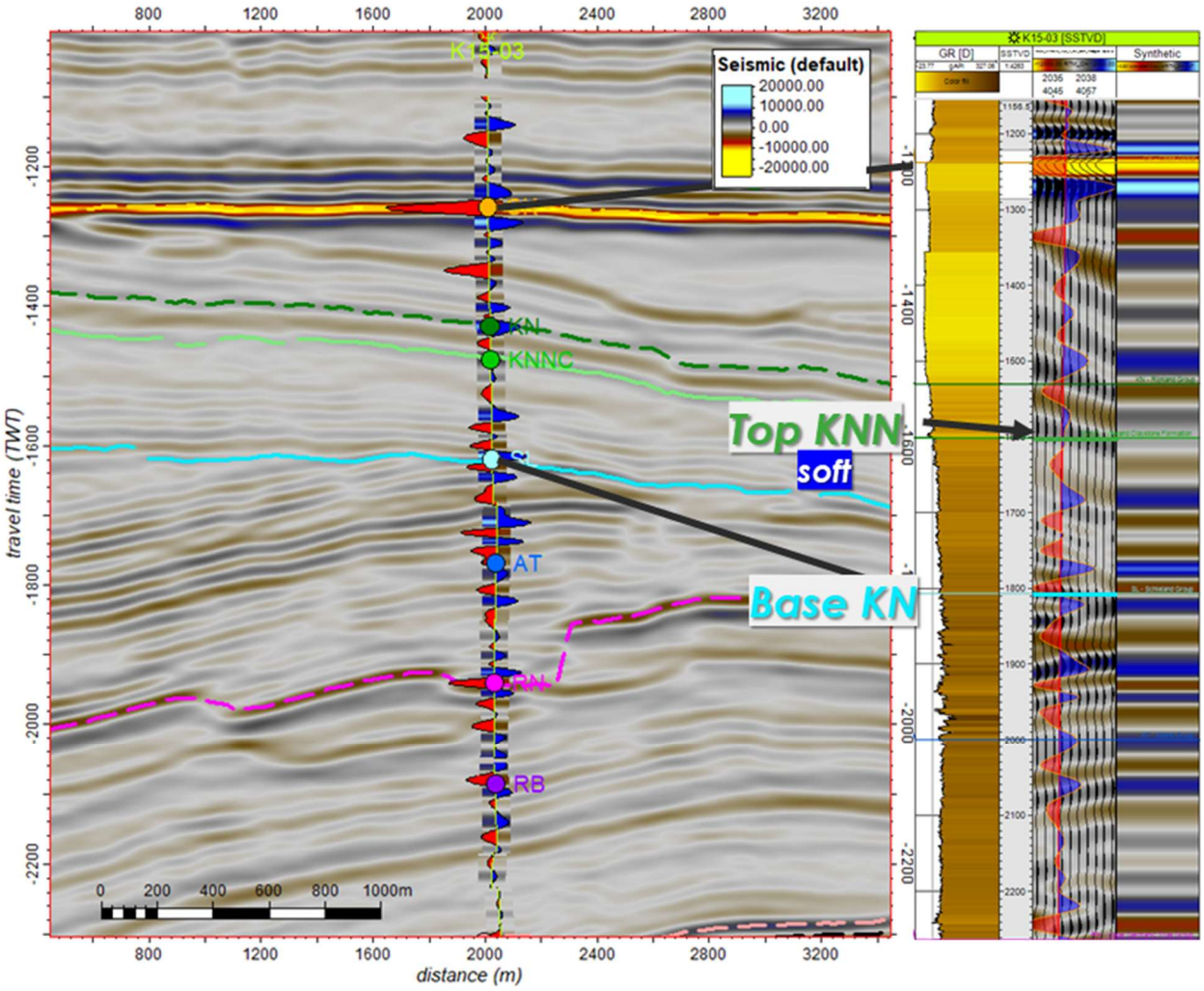

Figure 19: Seismic-to-well tie for well K15-03. The synthetic was calculated using density and sonic logs and tied to seismic in TWT. On the left, the synthetic is displayed in a single wiggle, on a bitmap with corresponding colors, on a cross-section of the TWT cube along the well trajectory. Dashed lines represent earlier interpretations on this same cube; in this figure the Top Upper Triassic, Base Chalk, and Base North Sea are interpreted. On the right, the well logs displayed are: GR, time OBN-seismic along the well with synthetic along the trajectory, and synthetic as a bitmap log.

To enable autotracking in an area as large as possible, interpretations of the Top Vlieland Vlieland Claystone were subdivided into two areas for the corresponding two characters (Fig. 20). Autotracking was done on a trough for a large part of the OBN-area; in the northwest, autotracking followed peaks. Between the two areas, the transition from one kick to another was interpolated. The interpolation was done within a polygon as well; boundaries of this polygon created a small artefact in final surface generation (see Fig. 22).

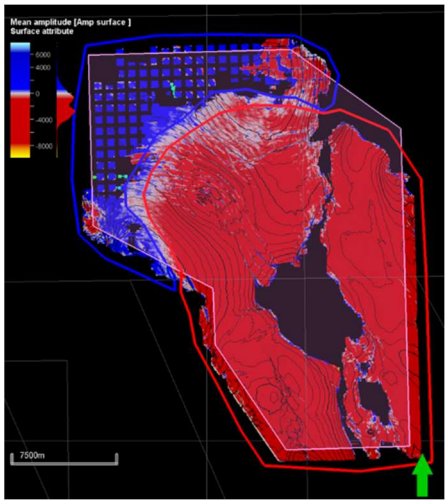

Figure 20: Amplitudes of a quick-look surface derived from Top Vlieland Claystone interpretations. The blue polygon comprises the area where Top Vlieland Claystone is a long soft kick. The red polygon encapsules area where the Top Vlieland is the lowest hard kick in a hard – soft – hard triplet. The polygons were used as boundaries for autotracking.

On the platform, the Top Vlieland Claystone has the same character as in the largest part of the basin (see Fig. 20). This was found by picking Top Vlieland Claystone in well L13-FH-101. Vlieland Sandstone is found in this well, though its GR-pattern and the well composite log suggested that the sand is less 'clean' (i.e. more clay-rich) than the sandstones found in the Kotter field area. This could be one of the causes for the weak synthetic seismic signal of the Top Vlieland Sandstone here. Other causes for a weak synthetic seismic signal could be the limited Vlieland Sandstone

thickness (24m). Furthermore, complexities in seismic-to-well tie arose from the position of the well in the vicinity of faults and the edge of the OBN-survey.

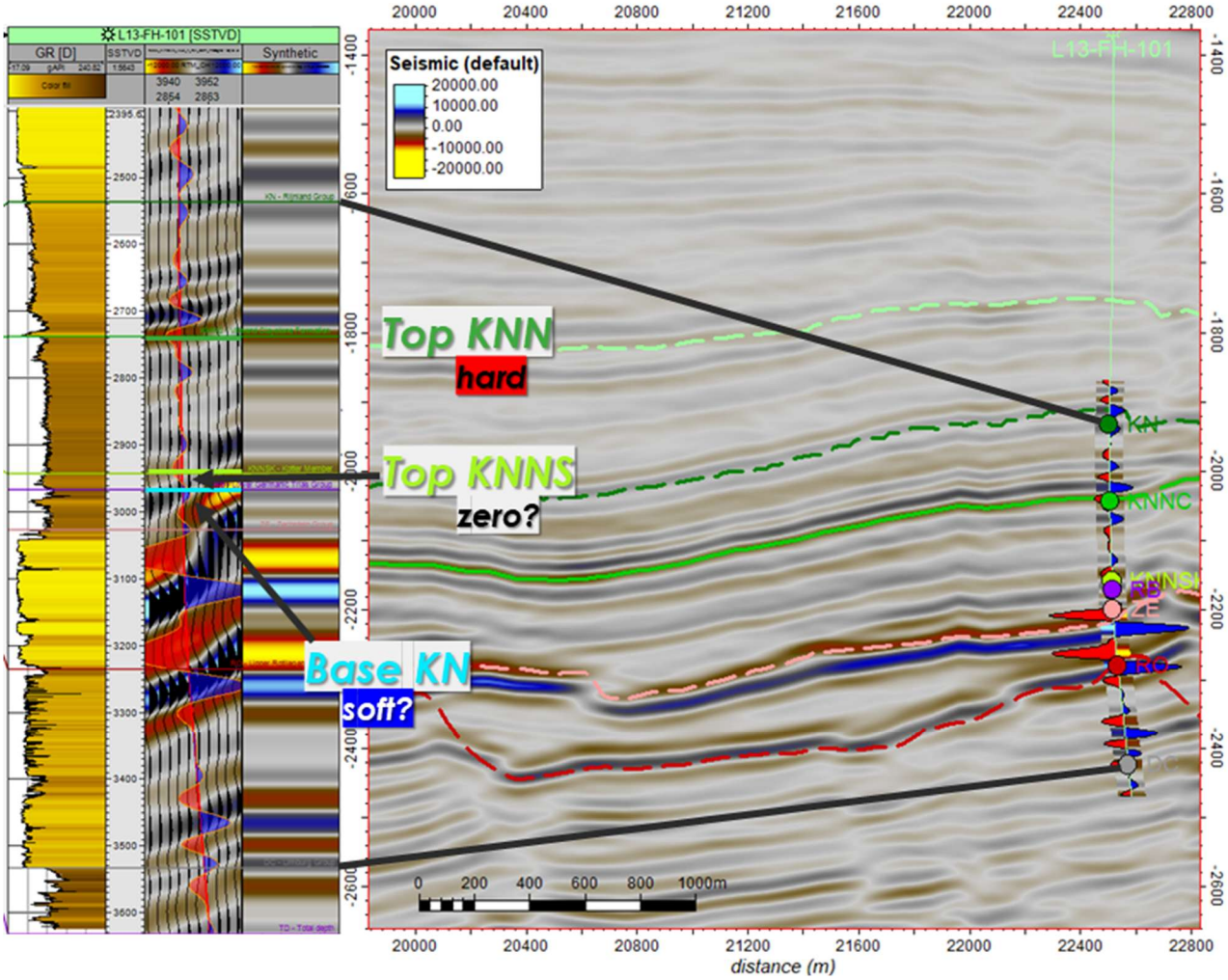

Figure 21: Seismic-to-well tie for well L13-FH-101. The synthetic was calculated using density and sonic logs and tied to seismic in TWT. On the left, the well logs displayed are: GR, time OBN-seismic along the well with synthetic along the trajectory, and synthetic as a bitmap log. On the right, the synthetic is displayed in a single wiggle, on a bitmap with corresponding colors, on a cross-section of the TWT cube along the well trajectory. Dashed lines represent earlier interpretations on this same cube; in this figure the Top Rotliegend, Top Zechstein, Base Chalk and an intra-Chalk horizon are interpreted.

4.4 Horizon Interpretation & Surface Generation

The results of horizon interpretation and subsequent surface generation are presented below. The basin inversion illustrated in the well panel in Figures 11 and 12 is also clearly visible from the depth map of the Top Vlieland Subgroup (Fig. 22): the basin (west) is generally shallower than the platform (east). In the south of the research area, the Top Vlieland Subgroup surface is truncated by the Base North Sea Group (white polygon in Fig. 22). In this area, the Base North Sea Group was used to replace the Top Vlieland Subgroup surface. At the easternmost edge of the basin, interpretation of the Top Vlieland (and all other horizons) is very hard due to the steep dip of reflectors. In this area (black polygon in Fig. 22), the Top Vlieland surface was generated parallel to the earlier interpreted Top Rijnland surface, guided by additional manual interpretations. In the north, a white area indicates that no Vlieland is present.

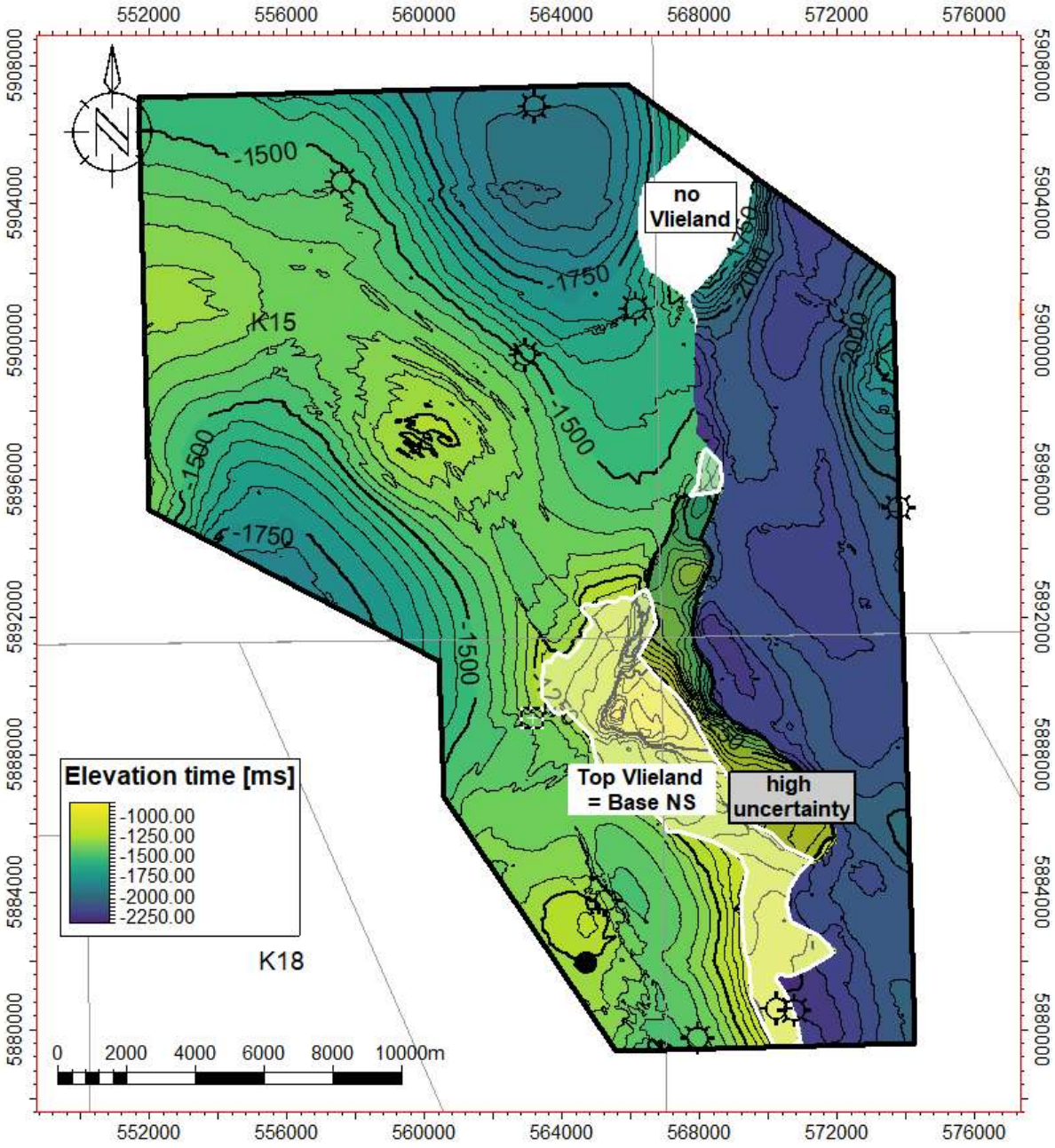

Figure 22: Depth of the Top Vlieland Subgroup surface in time (ms). Wells used for synthetic generation are indicated with same symbology as in Fig. 15. White polygons indicate areas where the Top Vlieland Subgroup is truncated by the Base North Sea Group. Black polygons indicate where the steeply dipping reflectors make interpretations unreliable. In the basin (west), the Top Vlieland Subgroup is higher than on the platform (east).

The base of the Vlieland Subgroup has a less strict stratigraphic definition than the Top Vlieland Subgroup. While Top Vlieland was almost everywhere interpreted as the interface between the Vlieland Claystone Fm. and the Holland Fm., the Base Vlieland Subgroup was interpreted as the interface between Vlieland and any unit subcropping below. Inherently, the character of this interface on seismic is laterally variable, as was expected (see Section 1.1). In some areas, reflectors of the underlying Schieland Group clearly end in a reflector (peak or trough). 3D autotracking was possible in these areas, supported by gridded horizon interpretation. No 3D autotracking was possible in regions where the Vlieland Subgroup is thinner, where the

dip of the reflectors is higher, or where the reflectors have lower amplitude. The Base Vlieland surface was generated from mostly manual interpretations in these areas (Fig. 23). On the platform, the 1D seismic character of the Base Vlieland Subgroup was determined in wells L13-FH-101 and L16-14 (see Table 3), however this 1D character could not be extended to interpret the Base Vlieland Subgroup on the platform. Therefore, the Base Vlieland Subgroup was set 198 m deeper than the Top Vlieland Claystone. Like the Top Vlieland Subgroup map, the Base Vlieland Subgroup map clearly illustrates the basin inversion.

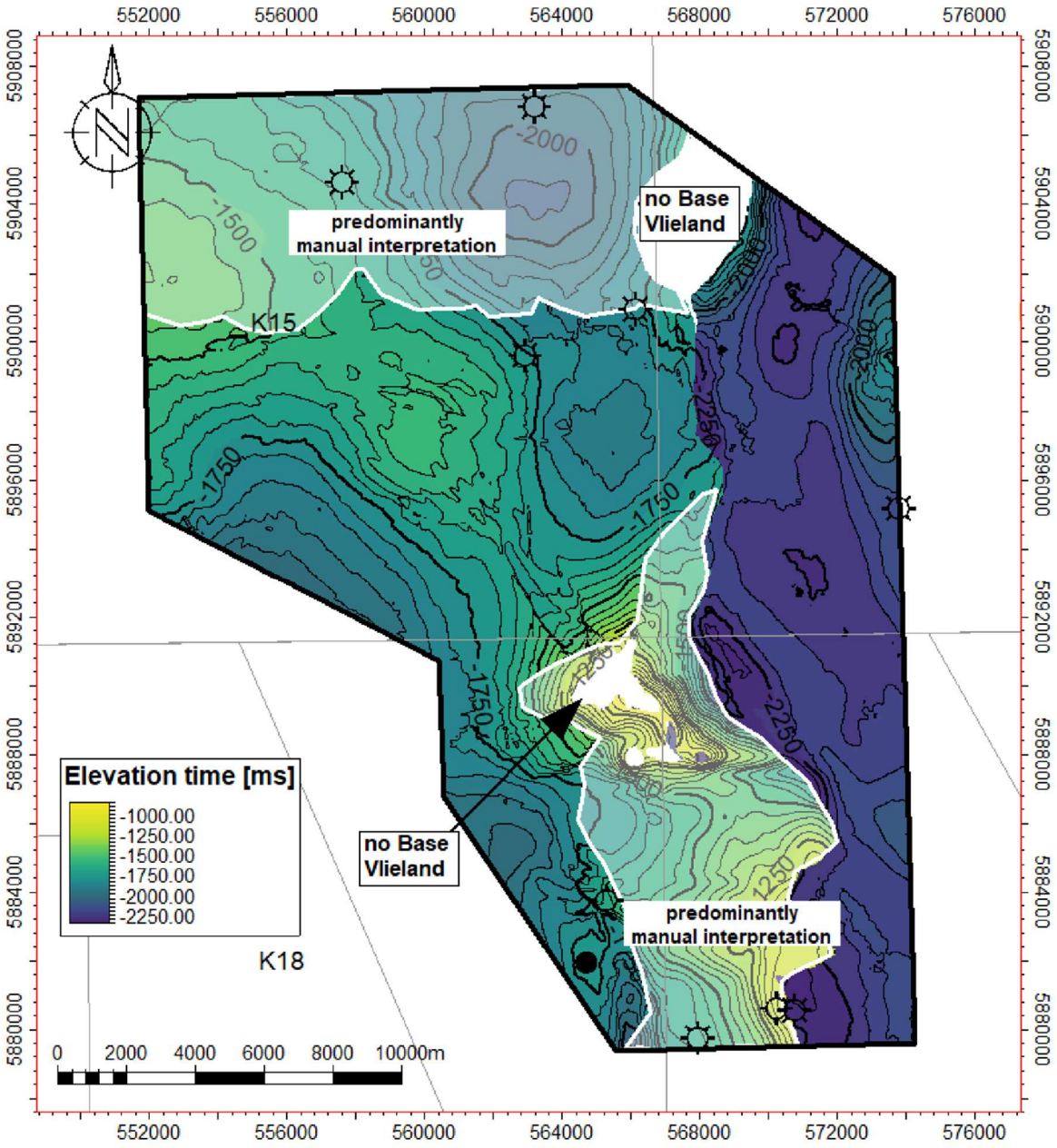

Figure 23: Depth of the Base Vlieland Subgroup surface in time (ms). Wells used for synthetic generation are indicated with same symbology as in Fig. 15. White polygons indicate areas where interpretations are mostly based on manual interpretation, due to highly variable or low-amplitude reflectors representing the Base Vlieland. As with the Top Vlieland Subgroup, the base Vlieland Subgroup surface higher in the basin (west) than on the platform (east).

The 1D seismic character of the Top Vlieland Sandstone was identified in multiple wells, yet the reflectors could not be extended throughout the research area (Fig. 24). In the area of the Kotter field, the Top Vlieland Sandstone horizon could be tracked (even 3D autotracked), but automated interpretations stopped at faults or at assumed seismic character changes (see Table 3, Fig. 17, Fig. 24). Attempts at (auto)tracking horizons were also made from starting points of other wells with synthetics in the Vlieland Sandstone Formation, yet the same problem in traceability was encountered. Where tracking was possible, horizon amplitude was calculated visualized, showing that amplitudes are higher around the Kotter field. The amplitudes decrease from the Kotter field to the north, suggesting a lower impedance contrast between KNNS and KNNC from south to north. It should be noted that outside the Kotter field, uncertainties are higher, weakening any conclusions about Top Sandstone amplitudes outside the Kotter field.

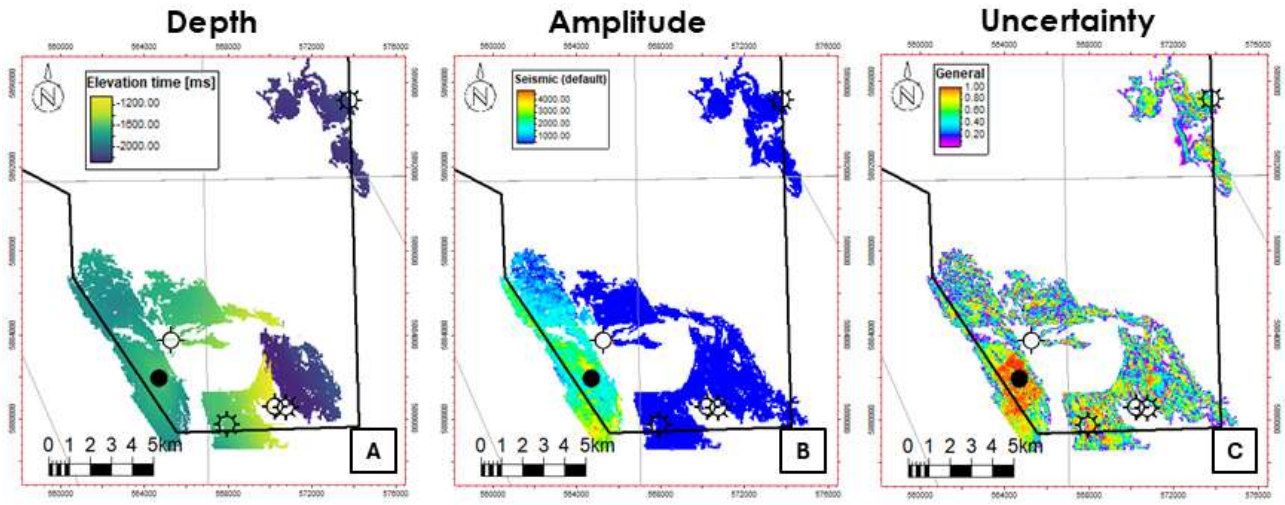

Figure 24: Top Vlieland Sandstone interpretations. The extent of horizon interpretation of Top Vlieland Sandstone is limited to the south and east of the research area. A) Elevation of horizon in time (ms), B) horizon amplitudes, C) horizon autotracking certainty.

With the Top Vlieland Subgroup surface being significantly more complete than the Top Vlieland Sandstone surface, the thickness of the full Vlieland Subgroup was calculated instead of the Vlieland Sandstone thickness (Fig. 25). This was done by subtracting the depths (in time) of the Top and Base Vlieland Subgroup, for the basin and platform respectively. The thickness maps of basin and platform were converted to depth using 'Velocity Model K' (see Section 2.2). The resulting thickness map shows a depocenter for Vlieland Subgroup in the southwest, and constant thickness of 198 m on the platform as expected from the methodology. Strong changes in thickness indicate presence and orientation of faults.

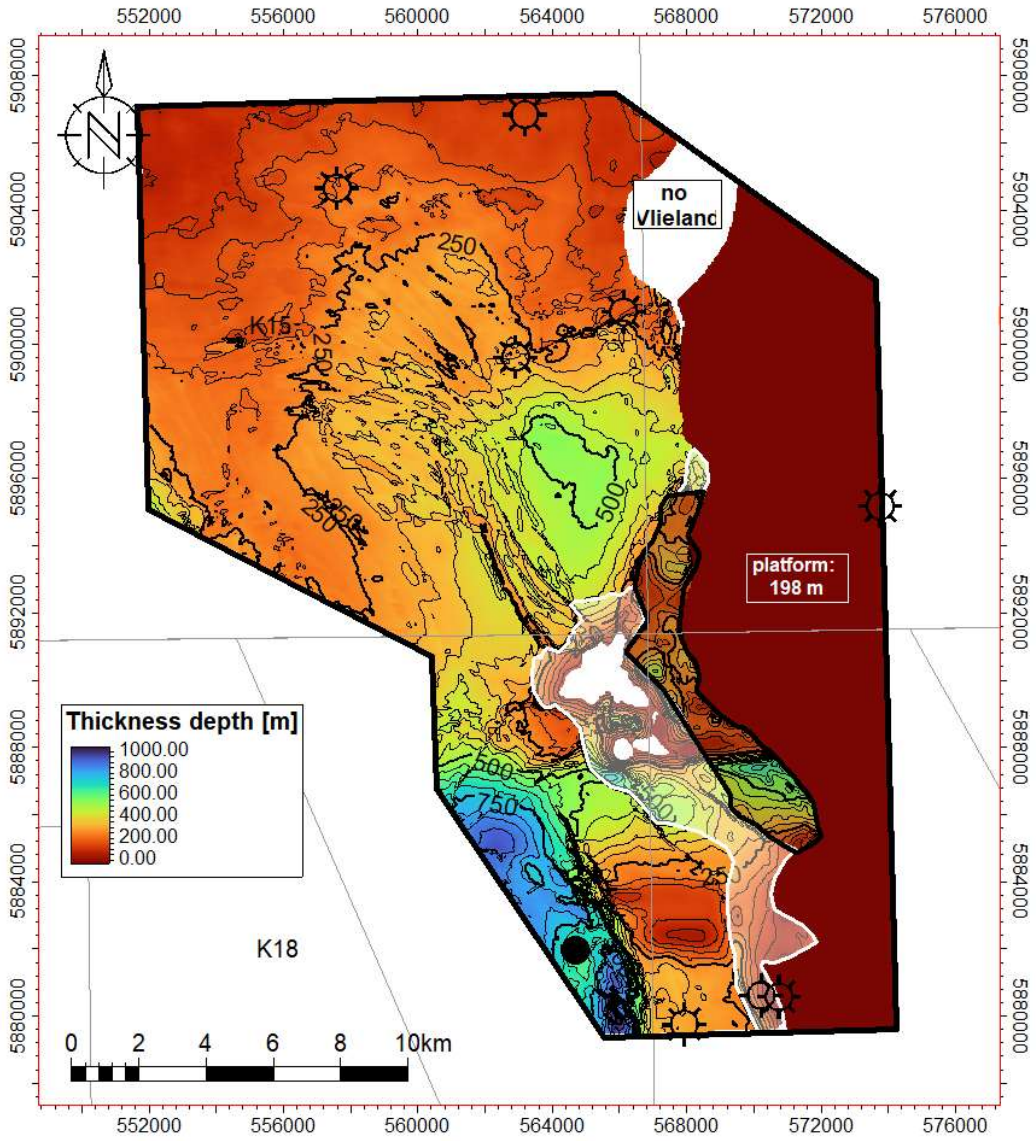

Figure 25: Vlieland Subgroup thickness map, calculated using surfaces of Top and Base Vlieland Subgroup derived from seismic interpretation. Wells used for synthetic generation are depicted in black, using symbology as in Figure 15. The Vlieland Subgroup has uniform thickness on the platform, because the Base Vlieland Subgroup was set 198 m lower than the Top Vlieland Subgroup here. The Vlieland Subgroup is thickest in the southwest.

5. 5. Discussion

5.1 Sandstone Thickness Proxy

Synthetic-seismics-informed horizon interpretation proved unsatisfactory for predicting Vlieland Sandstone presence on the full extent of the OBN-survey area (Fig. 24). To expand coverage of the Vlieland Sandstone thickness map, a proxy for Vlieland Sandstone thickness was therefore sought. Within the OBN-survey area, the area surrounding the Kotter field stood out: not only the sandstone thickness is expected to be highest here (Fig. 9), seismic interpretation showed that the full Vlieland Subgroup is also the thickest here (Fig. 25). Potentially, the Vlieland Subgroup thickness could guide in determining Vlieland Sandstone thickness.

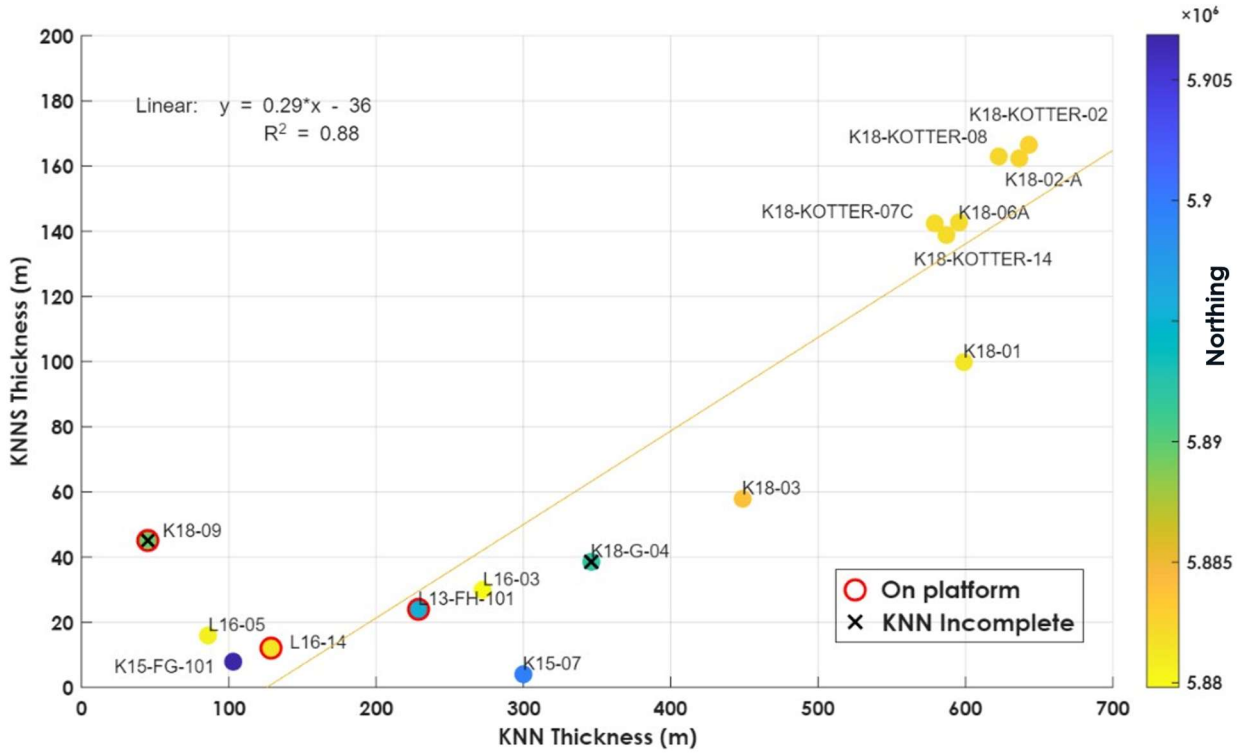

Figure 26: Empirical relationship of Vlieland Sandstone (KNNS) thickness and Vlieland Subgroup (KNN) thickness, for all wells in the OBN-survey area with KNNS thickness more than zero. Colors indicate the position of the wells with respect to the North. Points that represent wells with their Vlieland section outside the BFB are circled in red. Two wells are crossed out in black; these wells have an incomplete Vlieland section due to erosion of the topmost Vlieland Claystone. These wells are not in the dataset for the trendline. The linear trendline of scattered points is displayed in yellow, with corresponding equation and R^2 indicated on the top left of the graph.

An empirical relationship (R^2 of 0.88) was found between Vlieland Sandstone and Vlieland Subgroup thickness (note that only wells with a complete Vlieland Subgroup section were used) (Fig. 26). Wells with low Vlieland (Sandstone) thickness are in the north (blue colors), or on the platform (circled red), with exception of wells L16-05 and L16-03. The low KNNS and KNN thickness can be related to the position of these wells on a higher fault block than the K18 wells with thicker KNNS and KNN. On the scale of the OBN-survey area, the difference in Vlieland Sandstone well thickness appears to be related to I) the position of the well with respect to the Early Cretaceous SSE-directed transgression and to II) the position of the well with respect to faults – either the BFB bounding fault or smaller, intra-basin faults. This is in line with the findings from the well panels in Section 4.2.

The Vlieland Subgroup thickness was determined on seismic for the full research area: this thickness was inserted for *x* into the equation in Figure 26 to calculate *y* as the Vlieland Sandstone thickness. The calculated Vlieland Sandstone thickness was tied to well top thicknesses (Table 2) and clipped at values below zero, subsequently the thickness was summed with the depth of the Base Vlieland surface. This yielded a Top Vlieland Sandstone surface that could be inspected on seismic, beyond the areas where horizon (auto)tracking was possible (Fig. 24). The Top Sandstone surface in depth was converted to a TWT surface using 'Velocity Model K' (see Section 2.2), to enable comparison with the existing interpretations.

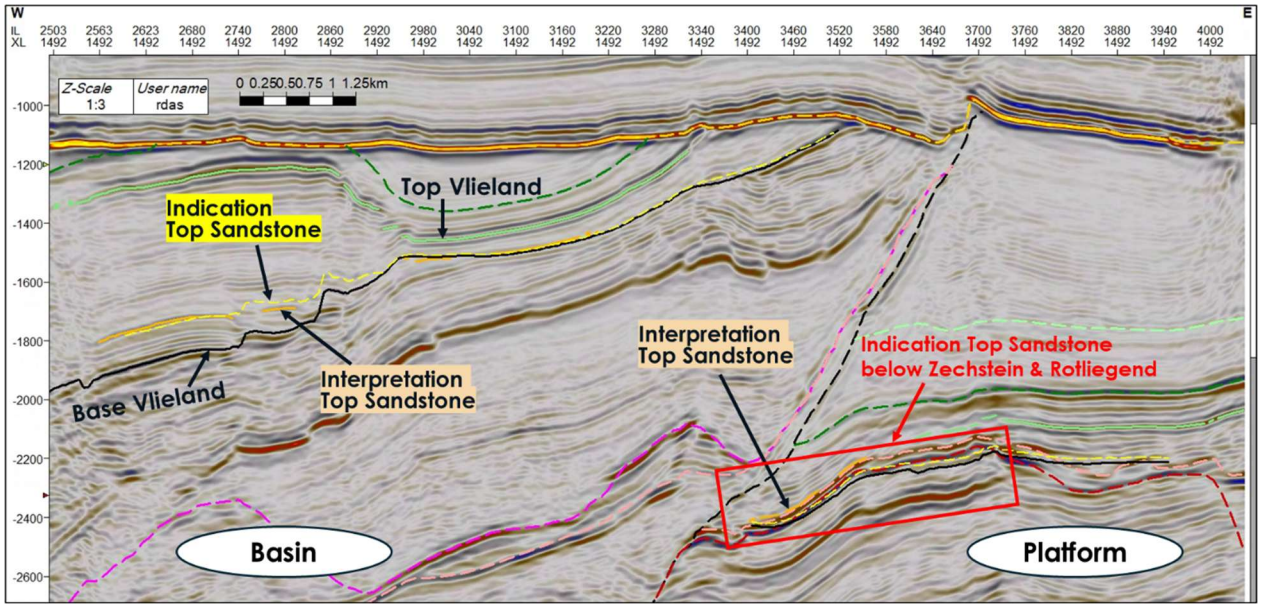

Figure 27: Comparison of the calculated Vlieland Sandstone surface to interpretations of this surface on XL 1492. The Vlieland Sandstone surface was calculated by inserting the thickness of the Vlieland Subgroup (from seismic interpretation) into an empirical equation (Fig. 26). The resulting thickness was tied to well tops and subsequently added to the Base Vlieland Surface to generate a Top Vlieland Sandstone surface on seismic. The resulting thickness matches interpretations well in the west (basin), but an erroneous surface is generated in the east (platform), below the top Zechstein and Rotliegend interpretations in coral and red, respectively.

The calculated Top Sandstone surface showed similarity to already interpreted Top Vlieland Sandstone surfaces on the basin side of the OBN-survey area (Fig. 27). On the platform, as expected, the Base Vlieland interpretation being exactly 198 m lower than the Top Vlieland interpretation, the calculated Top Vlieland was inadequate. The calculated Top Vlieland Sandstone surface was also inspected where no Top Sandstone horizon interpretation was considered possible (Fig. 28). The calculated sandstone thickness decreases to zero towards the west, in accordance with the Vlieland Subgroup becoming thinner in this direction. Interestingly, at the depth of the thicker calculated Vlieland Sandstone, a broad and clear soft kick is visible (Fig. 28B). Where the calculated sandstone is thinner, the blue colors of the soft kick amplitudes are less clear, indicating potentially a "pinch-out" of sandstone on seismic. It should be noted that in some areas, a very thin sandstone thickness was predicted by the model. For model thicknesses below 30m, inspection of the model on seismic was not possible.

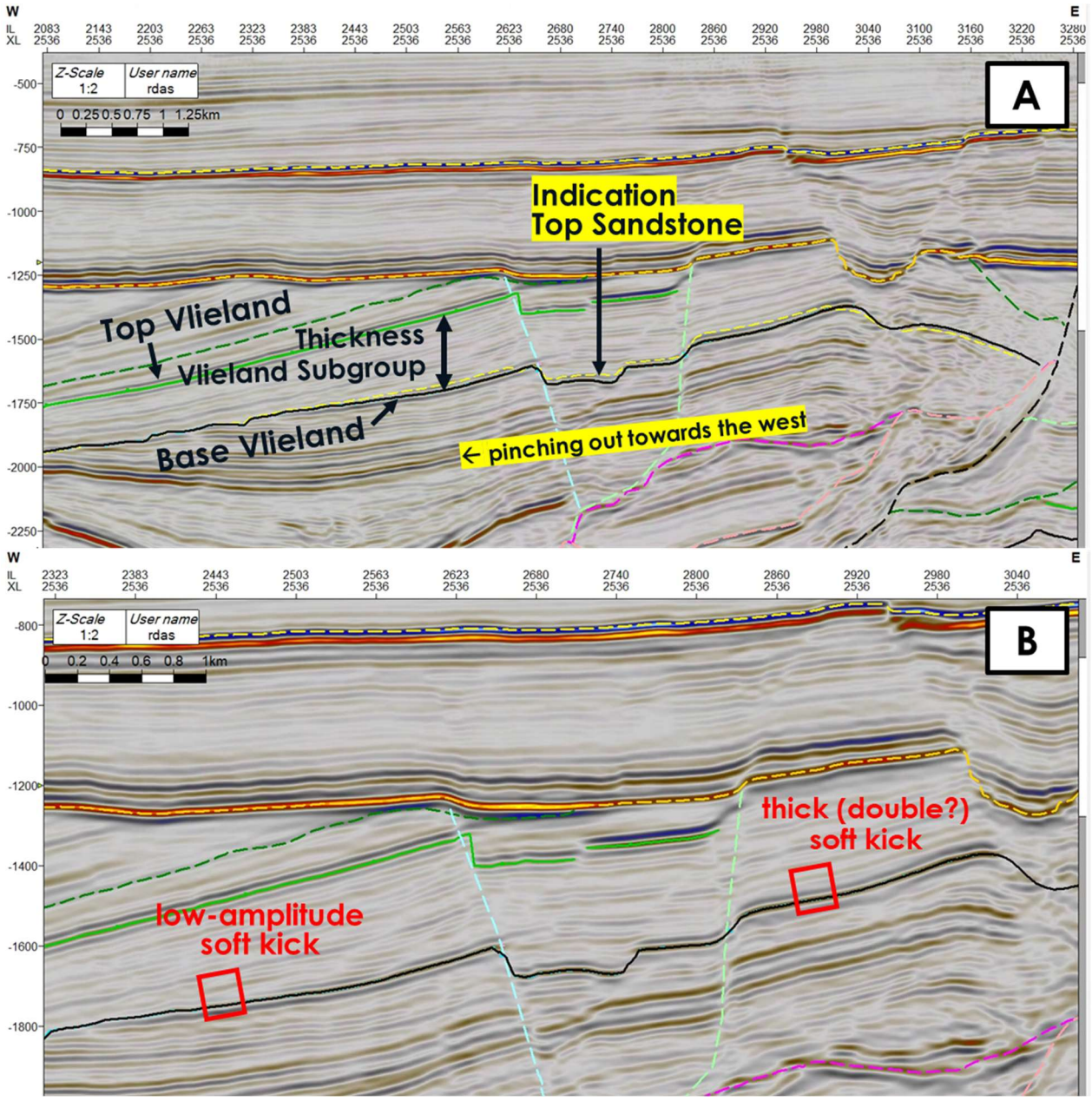

Figure 28: Inspection of the calculated Vlieland Sandstone surface on seismic, XL 2536. The Vlieland Sandstone surface was calculated by inserting the thickness of the Vlieland Subgroup (from seismic interpretation) into an empirical equation (Fig. 26). The resulting thickness was tied to well tops and subsequently added to the Base Vlieland Surface to generate a Top Vlieland Sandstone surface on seismic. The resulting thickness pinches out towards the west (A). The soft kicks that die out towards the west (above the Base Vlieland surface) could represent this pinch-out (B).

5.2 GDE

The Vlieland Sandstone Thickness map based on the empirical relationship (Fig. 26) – tied to well tops (Table 2) and to interpretations where possible (Fig. 24) – was used to create the GDE-map (GDE = Gross Depositional Environment) below. The map illustrates expected Vlieland Sandstone thickness, together with the factors that were found to influence the sandstone thickness. In accordance with the observation from the N-S well panel (Fig. 13), the GDE-map shows that the thickness of sandstone is influenced by tectonics: contour lines of the thickness map accumulate on fault lines, indicating a sharp change in thickness across the fault. The bounding fault of the BFB appears to not have the most impact on the change in sandstone thickness; instead, the smaller synthetic faults that populate the hanging wall account for the highest difference in Vlieland Sandstone thickness. This could suggest that the smaller intra-basin faults might have created the most accommodation space during the Early Cretaceous. The reason that the basin bounding fault is not the main divider for thicker vs. thinner KNNS deposits, could be because explained by Late Cretaceous inversion of a normal fault with less offset in the Lower Cretaceous. The largest thrust fault from the Alpine phase does not need to be the largest normal fault from the Cimmerian phase. Another factor that clearly influences sandstone thickness is the direction of the transgression. The thickness of sandstone decreases towards the north, in accordance with earlier studies on the SSE-directed transgression. On a smaller scale, it was observed that the amplitudes from the Kotter field become lower towards the north (Fig. 24B). This could imply that the impedance contrast between KNNS and KNNC lowers towards the north due to increased clay content in KNNS. This would imply that at smaller levels, a proximal – distal relationship can be distinguished as well.

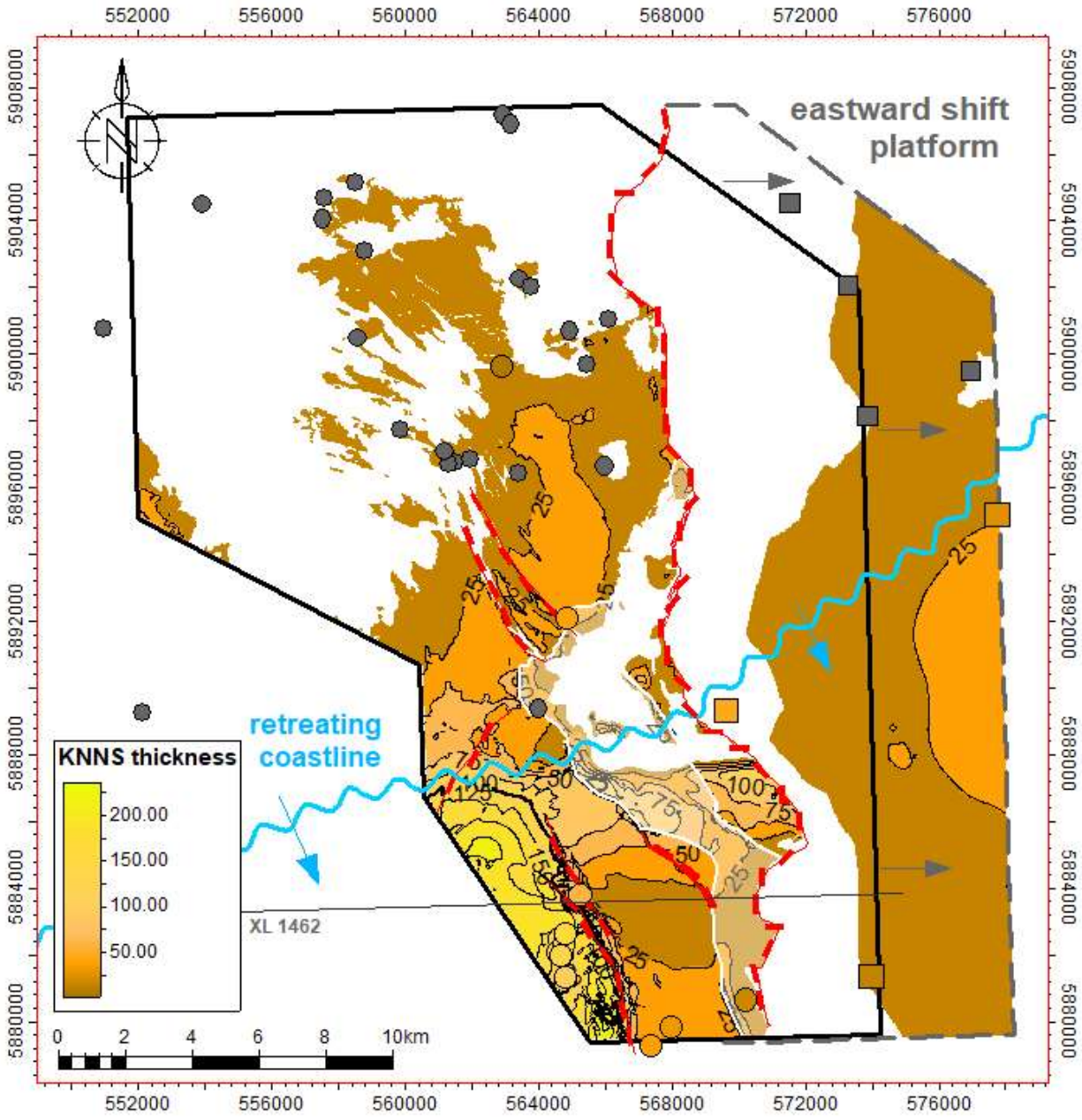

Figure 29: GDE-map, showing the calculated Vlieland Sandstone thickness, tied to interpretations and well tops. To avoid overlapping of interpretations, the calculated thickness on the platform is shifted 4km to the right, together with the corresponding wells (squares). Wells with KNNS mentioned are colored according to the thickness, wells without KNNS are indicated in grey. The cross-line of Figure 27 and Figure 30 is indicated in grey.

The Vlieland Sandstone thickness model can be used as a first indication for thief-zone, seal, or reservoir presence in the lowermost Vlieland Subgroup in the OBN-survey area. One should note however the uncertainties and the applicability of this map. Firstly, the modeled sandstone thickness on the platform is based on a less complete dataset than the sandstone thickness in the BFB, west of the bounding fault. Complexities in Base Vlieland Subgroup horizon interpretation resulted in the choice of setting the Base Vlieland parallel to the more reliable Top Vlieland horizon here. Therefore, the Vlieland Subgroup got uniform thickness, and no Vlieland Subgroup difference was inserted into the sandstone thickness model for the platform. Furthermore, only three wells could be used for tying the sandstone thickness on the platform.

Secondly, the map displays a gross sandstone thickness: intercalations of clays that can reduce the Net-to-Gross ratio were not considered in making this map. Porosities are also not considered – despite porosities from the Kotter field being higher (22 – 25%) than on the platform (13%)(TNO - GDN, 2026a) – meaning that storage potential can still vary for locations with the same modeled sandstone thickness. Thirdly, caution is required when applying the model outside this area. The Vlieland Sandstone thickness model was derived from an empirical relation of wells within the OBN-survey area only; using it in other areas could imply unjustified extrapolation of this relationship. It is recommended to further investigate the empirical relationship, e.g. finding populations with different trends, or determining whether the correlation is causal via a geological mechanism. Additionally, the Vlieland Sandstone formation is laterally heterogeneous between basins and intra-basin, which also decreases applicability of the model outside this area.

Though uncertainties of Vlieland (Sandstone) interpretations are clear, it should be noted that the OBN survey did enable interpretations on a scale that was not possible with the legacy surveys. It was already demonstrated that the new OBN survey provided added value for interpretation on unit scale (see Fig. 8). This study shows that on formation scale, the OBN survey improves resolution of interpretations as well. The cross-line from Fig. 27 is displayed again below, this time in comparison to the Terracube survey (Fig. 30). Reflectors of the Top Vlieland Claystone can be traced further down below the BFB bounding fault on the OBN survey, because penetration is deeper and reaches to the platform. Most importantly, however, faults within the Vlieland Subgroup in the basin, which proved important factors for determining Vlieland Sandstone thickness, can be better recognized on the OBN survey. For further investigation and mapping of the intra-basin faults on the OBN-survey, could add to an even better understanding of Vlieland Sandstone distribution.

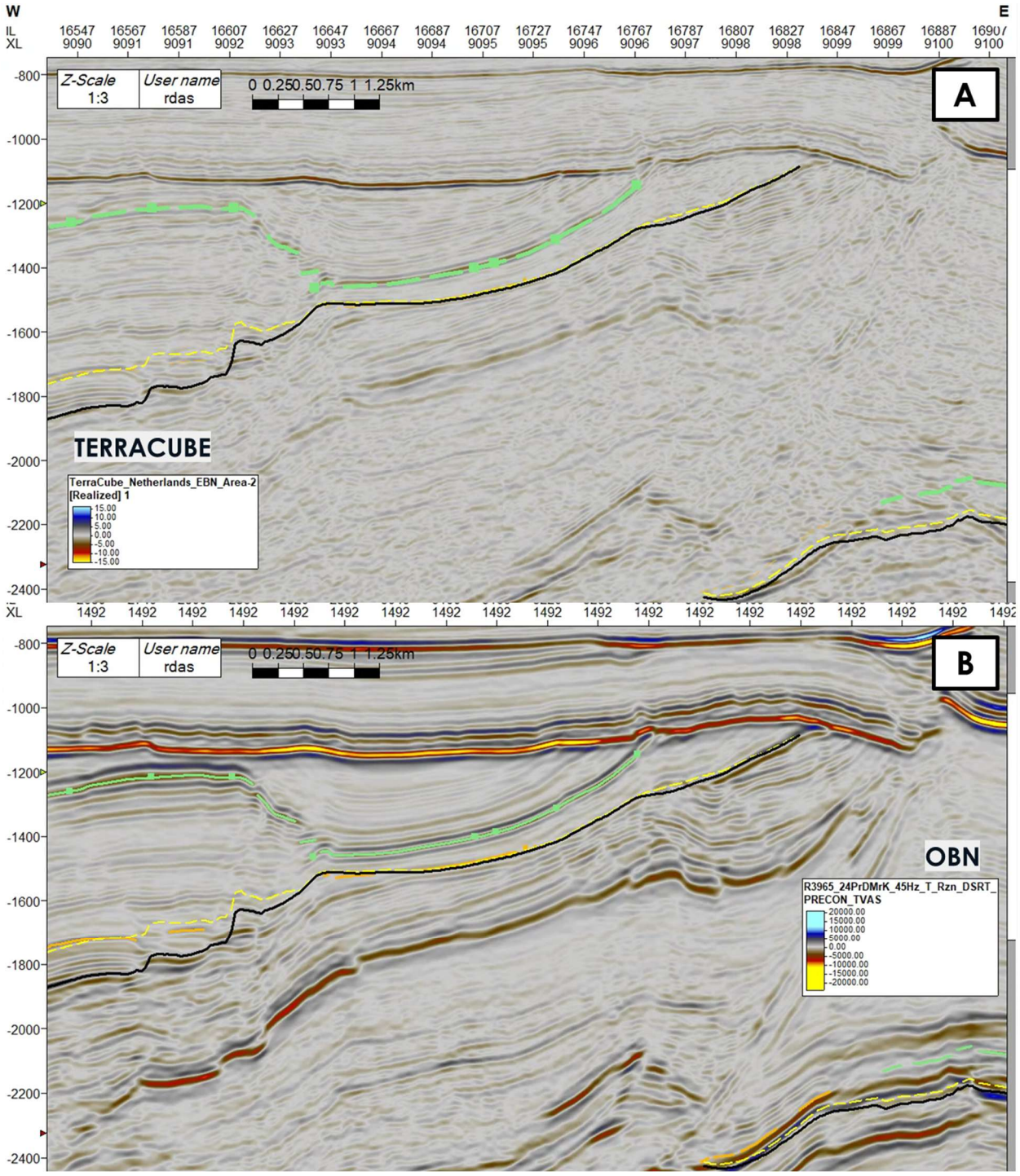

Figure 30: Comparison of Terracube (A) and OBN (B) imaging of the same cross-line. Key surfaces (Top KNN, Model Top KNNS, and Base KN) are indicated with the same symbology as in Figure 27. The OBN survey has better imaging of sub-fault reflectors and intra-basin faults within the Vlieland.

6. Conclusions

- The Vlieland Sandstone formation, represented by deepening sediments of an Early Cretaceous transgression, is known for its lateral heterogeneity between basins and even intra-basin. On a new, seismic survey, acquired using OBN (Ocean Bottom Node) technique, an attempt was made to characterize the Vlieland Sandstone Formation on seismic.

- The research area is geologically complex. Well panels and a subcrop map illustrate how normal faulting and subsequent basin inversion affected the completeness of stratigraphy on the scale of multiple stratigraphic units. A N-S well panel illustrates that both the transgression direction and subordinate faults (other than the basin bounding fault) affected deposition of Vlieland Sandstone. Biostratigraphic data imply that the lowermost Vlieland Subgroup has the same age throughout the research area, and that the Vlieland Subgroup is a complete record of the transgression when the top of the Vlieland Subgroup – e.g. the Base Holland Formation – is preserved.

- The top of the Vlieland Subgroup was successfully found on TWT 3D seismic, aided by generation of 10 synthetic seismograms. The base of the Vlieland Subgroup was successfully found in the basin, yet this horizon was too complex to follow on the platform, east of the basin bounding fault. The Base Vlieland surface was set parallel to the more reliable Top Vlieland surface, 198 m lower. Tracking the Top Vlieland Sandstone horizon was inhibited by its variable seismic character, identified both in synthetic seismograms and on 3D seismic. This hindered traceability across faults, from areas with seismic-to-well ties to areas without. In a large part of the research area, the Vlieland Sandstone formation has a thickness not visible on seismic.

- A model for sandstone thickness was developed by comparing Vlieland Sandstone to Vlieland Subgroup thickness in wells. A linear relationship was found with and R^2 of 0.88:

$$Thickness_{KNNS} = 0.29 * Thickness_{KNN} - 36$$

  The model was used to calculate sandstone thickness in the full extent of the OBN-area. This yielded a GDE map that successfully improved the existing thickness map of Vlieland Sandstone in this area, aided by seismic interpretation and detailed well analysis.

- The OBN-survey was found useful for better interpretation if relevant Vlieland horizons. Still, when using the presented seismic-informed sandstone thickness model for more local purposes, caution should be applied for model uncertainties, local sandstone properties, and the extent of model applicability.

7. References

1. Bouroullec, R., Verreussel, R. M. C. H., Geel, C. R., De Bruin, G., Zijp, M. H. A. A., Korösi, D., Munsterman, D. K., Janssen, N. M. M., & Kerstholt-Boegehold, S. J. (2018). Tectonostratigraphy of a rift basin affected by salt tectonics: synrift Middle Jurassic–Lower Cretaceous Dutch Central Graben, Terschelling Basin and neighbouring platforms, Dutch offshore. *Geological Society Special Publication*, *469*(1), 269–303. https://doi.org/10.1144/SP469.22
2. Bouroullec, R., Verreussel, R., Peeters, S., Kaliar, A., Ventra, D., Jones, D., Dieters, S., & Boter, E. (2024). DEVLI Project: Stratigraphy and Tectonostratigraphy of the Delflandand Vlieland subgroups, Upper Jurassic and Lower Cretaceous - Broad Fourteens Basin, West Netherlands Basin and neighbouring areas.
3. Chaves, A. C., Walker*, C., & McIntosh, S. (2011). *Autonomous Nodes – The Future of Marine Seismic Data Acquisition?* 1–6. https://doi.org/10.1190/SBGF2011-001
4. *Datacenter | NLOG*. (2025). https://www.nlog.nl/datacenter/
5. Deckers, J., & van der Voet, E. (2018). A review on the structural styles of deformation during Late Cretaceous and Paleocene tectonic phases in the southern North Sea area. *Journal of Geodynamics*, *115*, 1–9. https://doi.org/10.1016/J.JOG.2018.01.005
6. Den Hartog Jager, D. G. (1996). Fluviomarine sequences in the Lower Cretaceous of the West Netherlands Basin: correlation and seismic expression. *Geology of Gas and Oil under the Netherlands*, 229–241. https://doi.org/10.1007/978-94-009-0121-6_19
7. Gardner, G. H. F., Gardner, L. W., & Gregory, A. R. (1974). Formation velocity and density; the diagnostic basics for stratigraphic traps. *Geophysics*, *39*(6), 770–780. https://doi.org/10.1190/1.1440465
8. GEODE Metadata. (2023). *GEODE-Atlas Metadata: Play 3b KNNSK res thickness map*. GEODE-Atlas. https://geonetwork.geodeatlas.nl/geonetwork/srv/eng/catalog.search#/metadata/0a224045-58d3-4e23-b7fb-0e4bf802d916
9. Haq, B. U. (2018). JURASSIC SLV 2017 with online Supporting Material. *GSA Today*, *28*(1), 4–10. https://doi.org/10.1130/GSATG359A.1
10. Haskins, C. W., Lam, K. A., Love, C. F., Neville, R. S. W., Riley, L. A., Seymour, J. A., & Underwood, J. (1978). *Cities Service L/16 - 3 Dutch North Sea Well: Biostratigraphy of the Interval 1500m - 3351m*.
11. Head, R., & Simmons, M. (2020). *Exploration Handbook*. Haliburton Landmark.
12. Hooper, R. J., Goh, L. S., & Dewey, F. (1995). The inversion history of the northeastern margin of the Broad Fourteens Basin. *Geological Society Special Publication*, *88*, 307–317. https://doi.org/10.1144/GSL.SP.1995.088.01.17
13. Jager, J. de. (2007). *Geological development*. https://www.researchgate.net/publication/288910920_Geological_development
14. Jager, J. De. (2014). The discovery of the Fat Sand Play (Solling Formation, Triassic), Northern Dutch offshore – a case of serendipity. *Netherlands Journal of Geosciences*, *91*(4), 609–619. https://doi.org/10.1017/S0016774600000408
15. Jeremiah, J. M., Duxbury, S., & Rawson, P. (2010). Lower Cretaceous of the southern North Sea Basins: reservoir distribution within a sequence stratigraphic framework. *Netherlands Journal of Geosciences*, *89*(3–4), 203–237. https://doi.org/10.1017/S0016774600000706

16. KGG, M. van. (2025). Nationale Agenda Ondergrondse Waterstofopslag Het belang van waterstofopslag voor het energiesysteem.
17. Kombrink, H., Doornenbal, J. C., Duin, E. J. T., Den Dulk, M., Ten Veen, J. H., & Witmans, N. (2014). New insights into the geological structure of the Netherlands; results of a detailed mapping project. *Netherlands Journal of Geosciences*, *91*(4), 419–446. https://doi.org/10.1017/S0016774600000329
18. Lau, H. C., Ramakrishna, S., Zhang, K., & Radhamani, A. V. (2021). The Role of Carbon Capture and Storage in the Energy Transition. *Energy & Fuels*, *35*(9), 7364–7386. https://doi.org/10.1021/ACS.ENERGYFUELS.1C00032
19. Mavko, G., Mukerji, T., & Dvorkin, J. (2020). Empirical Relations. *The Rock Physics Handbook*, 474–524. https://doi.org/10.1017/9781108333016.008
20. Munsterman, D. K., Verreussel, R. M. C. K., Houben, A. J. P., & Kerstholt-Boegehold, S. J. (2012). *Biostratigraphy and organic geochemistry of well K18-G4*.
21. Peeters, S., Asschert, A., & Verweij, H. (2018). Towards a better understanding of the highly overpressured Lower Triassic Bunter reservoir rocks in the Terschelling Basin. *Geological Society Special Publication*, *469*(1), 223–236. https://doi.org/10.1144/SP469.13;WGROUP:STRING:PUBLICATION
22. Presentations DXD. (2024). Acquisition and Processing of the Southern North Sea's first OBN survey Operational/Technical challenges & achievements. www.sec.gov.
23. Schneider, A. C., Heimhofer, U., Heunisch, C., & Mutterlose, J. (2018a). From arid to humid – The Jurassic–Cretaceous boundary interval in northern Germany. *Review of Palaeobotany and Palynology*, *255*, 57–69. https://doi.org/10.1016/J.REVPALBO.2018.04.008
24. Schneider, A. C., Heimhofer, U., Heunisch, C., & Mutterlose, J. (2018b). The Jurassic–Cretaceous boundary interval in non-marine strata of northwest Europe – New light on an old problem. *Cretaceous Research*, *87*, 42–54. https://doi.org/10.1016/J.CRETRES.2017.06.002
25. Smit, J., van Wees, J. D., & Cloetingh, S. (2018). Early Carboniferous extension in East Avalonia: 350 My record of lithospheric memory. *Marine and Petroleum Geology*, *92*, 1010–1027. https://doi.org/10.1016/J.MARPETGEO.2018.01.004
26. Stille, H. (1926). Grundfragen der vergleichenden Tektonik. *Nature 1926 117:2936*, *117*(2936), 192–192. https://doi.org/10.1038/117192B0
27. Ten Veen, J. H., Van der Es, B., Boter, E., Van den Berg, A.-P., Dieters, S., De Haan, H., De Groot, L., Beintema, K., Peeters, S., & Foeken, J. (2023). *Play 3. Lower Cretaceous | GEODE Atlas*. https://www.geodeatlas.nl/pages/play-3-lower-cretaceous
28. Ten Veen, J., Vis, G., Jager, J., & Wong, T. (2025). Geological Development. In *Geology of the Netherlands* (2nd ed., 1). https://books.google.com/books?hl=nl&lr=&id=MG6LEQAAQBAJ&oi=fnd&pg=PT12&dq=geology+of+the+netherlands+2025&ots=J6POyPnNOm&sig=98gICkpGpaX03oTlUb6IaCNs2hM
29. TNO - GDN. (2025, December 11). *DINOloket KN*. Stratigrafische Nomenclator van Nederland. https://www.dinoloket.nl/stratigrafische-nomenclator/rijnland-groep
30. TNO - GDN. (2026a). *Datacenter | NLOG*. https://www.nlog.nl/datacenter/brh-overview
31. TNO - GDN. (2026b, January). *Rijnland Groep | DINOloket*. Stratigrafische Nomenclator van Nederland, TNO – Geologische Dienst Nederland. . https://www.dinoloket.nl/stratigrafische-nomenclator/rijnland-groep

32. Van Adrichem Kouwe, W. P. F., & Boogaert, H. A. (1993). Stratigraphic nomenclature of the Netherlands, revision and update by RGD and NOGEPA. *Stratigraphic Nomenclature of the Netherlands, Revision and Update by RGD and NOGEPA*, (50), pag. mult.
33. Verreussel, R. M. C. H., Bouroullec, R., Houben, A. J. P., & Munsterman, D. K. (2025). Late Jurassic – Early Cretaceous. *Geology of the Netherlands*. https://doi.org/10.5117/9789463728362_CH07
34. Verreussel, R. M. C. H., Bouroullec, R., Munsterman, D. K., Dybkjær, K., Geel, C. R., Houben, A. J. P., Johannessen, P. N., & Kerstholt-Boegehold, S. J. (2018). Stepwise basin evolution of the Middle Jurassic–Early Cretaceous rift phase in the Central Graben area of Denmark, Germany and The Netherlands. *Geological Society Special Publication*, *469*(1), 305–340. https://doi.org/10.1144/SP469.23
35. Willems, C. J. L., Vondrak, A., Mijnlieff, H. F., Donselaar, M. E., & Van Kempen, B. M. M. (2020). Geology of the Upper Jurassic to Lower Cretaceous geothermal aquifers in the West Netherlands Basin – an overview. *Netherlands Journal of Geosciences*, *99*, e1. https://doi.org/10.1017/NJG.2020.1
36. Woodcock, N. H. ., & Strachan, R. A. . (2015). *Geological history of Britain and Ireland*. https://books.google.com/books/about/Geological_History_of_Britain_and_Irelan.html?hl=nl&id=HRLdyp5_Z48C
37. Zanella, E., & Coward, M. P. (2003). Structural Framework. In *The Millenium Atlas: petroleum geology of the central and northern North Sea*. The Geological Society of London. https://www.researchgate.net/publication/281611517_Structural_framework
38. Ziegler, P. A., & Cloetingh, S. (2004). Dynamic processes controlling evolution of rifted basins. *Earth-Science Reviews*, *64*(1–2), 1–50. https://doi.org/10.1016/S0012-8252(03)00041-2